

hep-ph/0107048  
 TUM-HEP-419/01  
 IFT-01/17

July 2001

# $\Delta M_s/\Delta M_d$ , $\sin 2\beta$ and the angle $\gamma$ in the Presence of New $\Delta F = 2$ Operators

Andrzej J. Buras<sup>1</sup>, Piotr H. Chankowski<sup>2</sup>,  
 Janusz Rosiek<sup>1,2</sup> and Łucja Sławianowska<sup>2</sup>

<sup>1</sup> Physik Department, Technische Universität München,  
 D-85748 Garching, Germany

<sup>2</sup> Institute of Theoretical Physics, Warsaw University  
 Hoża 69, 00-681 Warsaw, Poland

## Abstract

We present formulae for the mass differences  $\Delta M_d$  and  $\Delta M_s$  in the  $\bar{B}_{d,s}^0$ - $B_{d,s}^0$  systems and for the CP violation parameter  $\varepsilon$  which are valid in minimal flavour violation models giving rise to new four-fermion  $\Delta F = 2$  operators. Short distance contributions to  $\Delta M_s$ ,  $\Delta M_d$  and  $\varepsilon$  are parameterized by three *real* functions  $F_{tt}^s$ ,  $F_{tt}^d$  and  $F_{tt}^\varepsilon$ , respectively ( $F_{tt}^s = F_{tt}^d = F_{tt}^\varepsilon$  holds only if the Standard Model  $(V-A) \otimes (V-A)$  operators dominate). We present simple strategies involving the ratio  $\Delta M_s/\Delta M_d$ ,  $\sin 2\beta$  and  $\gamma$  that allow to search for the effects of the new operators. We point out that their sizable contributions to the ratio  $\Delta M_s/\Delta M_d$  would in principle allow  $\gamma$  to be larger than  $90^\circ$ . Constraints on the functions  $F_{tt}^i$  imposed by the present (and future) experimental data are also discussed. As an example we show that for large  $\tan \bar{\beta} \equiv v_2/v_1$  and  $H^+$  not too heavy,  $F_{tt}^s$  in the MSSM with heavy sparticles can be substantially smaller than in the SM due the charged Higgs box contributions and in particular due to the growing like  $\tan^4 \bar{\beta}$  contribution of the double penguin diagrams involving neutral Higgs boson exchanges. As a result the bounds on the function  $F_{tt}^s$  can be violated which allows to exclude large mixing of stops. In this scenario the range of  $\sin 2\beta$  following from  $\varepsilon$  and  $\Delta M_d$  is identical to the SM ones ( $0.5 < \sin 2\beta < 0.8$ ). On the other hand  $\gamma$  following from  $\Delta M_s/\Delta M_d$  is lower.

# 1 Introduction

The determination of the CKM parameters and of the related unitarity triangle (UT) are the hot topics in particle physics [1]. In this context a clean measurement of the angle  $\beta$  in the unitarity triangle through the time dependent CP asymmetry,  $a_{\psi K_S}(t)$ , in  $B_d^0(\bar{B}_d^0) \rightarrow \psi K_S$  decays is very important.

In the Standard Model (SM)

$$a_{\psi K_S}(t) \equiv -a_{\psi K_S} \sin(\Delta M_d t) = -\sin 2\beta \sin(\Delta M_d t), \quad (1.1)$$

thereby allowing direct extraction of  $\sin 2\beta$ . The most recent measurements of  $a_{\psi K_S}$  from the BaBar and Belle Collaborations give

$$a_{\psi K_S} = \begin{cases} 0.59 \pm 0.14 \pm 0.05 & (\text{BaBar}) [2] \\ 0.99 \pm 0.14 \pm 0.06 & (\text{Belle}) [3]. \end{cases} \quad (1.2)$$

Combining these results with earlier measurements at CDF ( $0.79^{+0.41}_{-0.44}$ ) [4] and by the ALEPH collaboration ( $0.84^{+0.82}_{-1.04} \pm 0.16$ ) [5] would give the grand average

$$a_{\psi K_S} = 0.79 \pm 0.10, \quad (1.3)$$

but in view of the fact that BaBar and Belle results are not fully consistent with each other we believe that a better description of the present situation is  $a_{\psi K_S} = 0.80 \pm 0.20$ .

Similarly important for the determination of the unitarity triangle will be the measurement of the ratio of the mass differences in the  $\bar{B}_{d,s}^0$ - $B_{d,s}^0$  systems,  $\Delta M_s/\Delta M_d$ . The experimental values of  $\Delta M_d$  and  $\Delta M_s$  read [6]

$$\Delta M_d = (0.487 \pm 0.009)/ps, \quad \Delta M_s \geq 15.0/ps, \quad (1.4)$$

implying

$$\frac{\Delta M_s}{\Delta M_d} \geq 30/ps, \quad (1.5)$$

which is compatible with the SM expectations. Because theoretically this ratio is considerably cleaner than  $\Delta M_s$  and  $\Delta M_d$  themselves, its precise measurement will have an important impact on the determination of the unitarity triangle and on the tests of the SM and its various extinctions. As emphasized in [1, 7, 8, 9, 10] this impact will be even stronger in conjunction with the measurement of  $a_{\psi K_S}$ . It is therefore exciting that  $\Delta M_s/\Delta M_d$  should be measured already this year in Run II at Fermilab, while improvements of the  $a_{\psi K_S}$  measurements are expected from BaBar, Belle, CDF, D0 and, at later stages, from BTeV and LHC experiments.

The result (1.3) for  $a_{\psi K_S}$  should be compared with the value of  $\sin 2\beta$  obtained from the analyses of the unitarity triangle in the framework of the Standard Model (SM) [1, 7, 11] that center around  $(\sin 2\beta)_{\text{SM}} \approx 0.70$  with estimated errors ranging from 0.07 to 0.24. Clearly in view of large experimental error in (1.3) and the considerable uncertainty in the error estimates of  $(\sin 2\beta)_{\text{SM}}$ , the SM fits are compatible with the experimental value of  $a_{\psi K_S}$ . The small value of  $a_{\psi K_S}$  found earlier by the BaBar collaboration [12] has not been confirmed by most recent data. On the other hand, the large value of  $a_{\psi K_S}$  measured by the Belle collaboration may be suggestive of new physics contributions to  $B_d^0(\bar{B}_d^0) \rightarrow \psi K_S$ ,  $\bar{B}_{d,s}^0$ - $B_{d,s}^0$  mixing,  $\bar{K}^0$ - $K^0$  mixing and/or the parameter  $\varepsilon$  measuring CP violation in the  $\bar{K}^0$ - $K^0$  mixing. Thus the analyses [10], [13]–[21] of new contributions done in the context of small  $a_{\psi K_S}$  value reported by BaBar [12] could still be relevant if properly reformulated. Such new contributions could modify not only the relation between  $a_{\psi K_S}$  and  $\sin 2\beta$  in (1.1) but also the value of  $\sin 2\beta$  obtained from the fits of the unitarity triangle.

In general models of new physics potentially contributing to  $a_{\psi K_S}$ ,  $\Delta M_{d,s}$  and/or  $\varepsilon$  fall into the two following broad classes [1]:

- Models in which the CKM matrix remains the unique source of both, flavour and CP violation. The effects of this source are however modified by the new interaction vertices (of new particles) in which the CKM matrix elements appear.
- Models with entirely new sources of flavour and/or CP violation.

The first class can be conveniently further subdivided into the so-called MFV models [22, 9] and the generalized MFV models (GMFV).

The characteristic feature of the MFV models (MVF scenarios of new physics) is the strong dominance in their low energy effective Hamiltonian of the same operators that occur in the low energy effective Hamiltonian of the SM. In such models the formula (1.1) remains valid and the relation between the ratio  $\Delta M_s/\Delta M_d$  and the length of one side of the unitarity triangle,  $R_t$ , is as in the SM: it remains independent of the parameters of the particular model. Thus, for this class of models the unitarity triangle is universal [9]. The distinction between different models of this class can then be made through the study of  $\varepsilon$  and  $\Delta M_d$  which in contrast to  $a_{\psi K_S}$  and  $\Delta M_s/\Delta M_d$  do depend explicitly on new physics contributions. A detailed analysis of the profile of the UT in supersymmetric scenarios of this class can be found in [7]. Other discussions of the MFV models can be found in [19, 20, 23].

The GMFV models generalize the MFV models by allowing for significant contributions of the nonstandard operators in the effective low energy Hamiltonian. In this class of models the formula (1.1) is still valid but the relation between  $\Delta M_s/\Delta M_d$  and  $R_t$  is

modified. Hence,  $R_t$  determined from the measured ratio  $\Delta M_s/\Delta M_d$  does depend on the parameters of the model.

While the presence of new CP violating phases in  $\bar{B}_{d,s}^0$ - $B_{d,s}^0$  mixing and  $\bar{K}^0$ - $K^0$  mixing could turn out to be necessary to explain the future precise value of  $a_{\psi K_S}$ , it is important to investigate first the scenarios that do not invoke new sources of flavour and/or CP violation. It is therefore useful to analyze first MFV and GMVF models that are more constrained than the more general scenario mentioned above.

It turns out that in the MFV models there exists an *absolute* lower bound on  $\sin 2\beta$  [10] that follows from the interplay of  $\Delta M_d$  and  $\varepsilon$  and depends mainly on  $|V_{cb}|$ ,  $|V_{ub}/V_{cb}|$  and the non-perturbative parameters  $\hat{B}_K$ ,  $F_{B_d}\sqrt{\hat{B}_{B_d}}$  entering the analysis of the unitarity triangle. An updated conservative lower bound on  $\sin 2\beta$  obtained by scanning independently all relevant input parameters reads [1]

$$(\sin 2\beta)_{\min} = 0.42 . \quad (1.6)$$

As analyzed in [10, 1], this bound could be considerably improved when the values of  $|V_{cb}|$ ,  $|V_{ub}/V_{cb}|$ ,  $\hat{B}_K$ ,  $F_{B_d}\sqrt{\hat{B}_{B_d}}$ , will become better known or if  $\Delta M_s$  is measured so that the ratio  $\Delta M_s/\Delta M_d$  can be used, along with the non-perturbative parameter  $\xi$ , to determine the length of one side of the UT. The lower bound (1.6) is fully consistent with the experimental data but as the latter are not yet very precise it could prove useful when the knowledge of  $|V_{cb}|$ ,  $|V_{ub}/V_{cb}|$ ,  $\hat{B}_K$ ,  $F_{B_d}\sqrt{\hat{B}_{B_d}}$ ,  $\Delta M_s$  and  $\xi$  improves. Note that the bound (1.6) allows values of  $\sin 2\beta$  that are slightly smaller than the ones obtained from the fits to the unitarity triangle within the SM,  $(\sin 2\beta)_{\text{SM}} > 0.5$ . In view of the unexpectedly high value of  $a_{\psi K_S}$  found by the Belle collaboration [3], more interesting at present appears the upper bound on  $\sin 2\beta$  in MFV models that reads [8, 23]

$$(\sin 2\beta)_{\max} = 2R_b\sqrt{1 - R_b^2} . \quad (1.7)$$

Here  $R_b$  is the lenght of one side of the unitarity triangle (see fig. 1) given in terms of  $|V_{ub}/V_{cb}|$  in eq. (2.12). With the input parameters specified in table 1, one obtains  $(\sin 2\beta)_{\max} = 0.82$  that is fully consistent with the BaBar result [2] but appears to be violated by the Belle result [3]. We will return to this issue in the course of this paper. The natural next step is to exploit GMVF models. In the present paper we would like to make this step and present general formulae relevant for the analysis of the unitarity triangle and  $\sin 2\beta$  in the GMVF models.

Examples of the MFV models are the Two Higgs Doublet Models II (2HDM(II)) and the MSSM, in which sfermion mass squared matrices are aligned with the corresponding fermion mass matrices and the CP violating phases of the gaugino masses,  $\mu$  and  $A$

parameters are all set to zero, provided the ratio of the vacuum expectation values of the two Higgs doublets,  $v_2/v_1 \equiv \tan \bar{\beta}$  is not too large. It is well known [24, 25] that in both these models the contribution of light charged Higgs boson and/or (in the case of supersymmetry) charginos and stops to the Wilson coefficient of the standard  $(V - A) \otimes (V - A)$  operator can significantly enhance the  $tW^\pm$  contribution to  $\Delta M_s$ ,  $\Delta M_d$  and  $\varepsilon$ . In this paper we show that for large  $\tan \bar{\beta} \equiv v_2/v_1$  both models become GMFV models. In particular in the MSSM in the limit  $M_W \lesssim M_{H^+} \ll M_{\text{sparticle}}$ , which we consider here for simplicity, we find that:

- There can be significant contributions to  $\Delta M_s$  from the charged Higgs box diagrams (growing like  $\tan^2 \bar{\beta}$  at the 1-loop level and faster after including leading higher order corrections) and, growing as  $\tan^4 \bar{\beta}$ , contributions arising from the double penguin diagrams involving the neutral Higgs scalars. Compared to the contribution of the extended Higgs and chargino/stop sectors relevant for low  $\tan \bar{\beta}$ , the interesting feature of all these new contributions is their sign which is opposite to the standard  $tW^\pm$  box contribution.
- Compared to  $\Delta M_s$ , the corresponding contributions to  $\Delta M_d$  and  $\varepsilon$  are suppressed by the quark mass ratios  $m_d/m_s$  and  $m_d/m_b$ , respectively.
- Consequently, in this scenario  $\sin 2\beta$  cannot deviate significantly from its SM value, i.e. the lower bound (1.6) can never be reached.
- Present experimental data strongly limit large mixing of stops if their mass difference is large compared to the electroweak scale.
- If  $a_{\psi K_S}$  is found below 0.5 or above 0.82 this particular supersymmetric scenario will be disfavoured (together with the SM). If  $a_{\psi K_S} \approx 0.7$  this scenario can lead to the  $\gamma$  angle slightly smaller (depending on the measured value of  $\Delta M_s$ ) than in the SM.

The full MSSM with large  $\tan \bar{\beta}$ , including the effects of light sparticles, will be analyzed in the forthcoming paper [26].

Our paper is organized as follows. In section 2 we generalize the MFV formulae of [10, 9, 1] to GMFV models. While in MFV models the new physics short distance contributions to  $\bar{B}_{d,s}^0$ - $B_{d,s}^0$  mixing and  $\varepsilon$  can be described by only a single function  $F_{tt}$ , the transition to the GMFV models (in which new operators contribute) requires the introduction of three *real* functions  $F_{tt}^d$ ,  $F_{tt}^s$  and  $F_{tt}^\varepsilon$ . We present simple strategies involving the ratio  $\Delta M_s/\Delta M_d$ ,  $\sin 2\beta$  and the angle  $\gamma$  that allow to search for the effects caused by new operators (sec. 2.3) and discuss model independent bounds on the functions  $F_{tt}^{s,d,\varepsilon}$  which follow from the present and future experimental data (sec. 2.4). We also point out

that in this class of models the function  $F_{tt}^s$  can be directly measured through  $\Delta M_s$  and that the angle  $\gamma$  could be larger than  $90^\circ$ . The formulae necessary to express the functions  $F_{tt}^{s,d,\varepsilon}$  directly in terms of the Wilson coefficients of the four-fermion operators are collected in Section 3. The 2HDM(II) and the MSSM with large  $\tan\bar{\beta} \equiv v_2/v_1$  and heavy sparticles are discussed in Section 4. We give complete formulae for the one loop contribution of the box diagrams involving charged Higgs bosons and derive simple approximate formulae describing the dominant effects of the double penguin diagrams. Consequences of their large contribution and implications of the bounds presented in sec. 2.4 are also discussed. We conclude in Section 5.

## 2 Basic Formulae

### 2.1 Effective Hamiltonian in GMVF Models

The effective weak Hamiltonian for  $\Delta F = 2$  transitions in the GMVF models can be written as follows

$$H_{\text{eff}}^{\Delta F=2} = \frac{G_F^2 M_W^2}{16\pi^2} \sum_i V_{\text{CKM}}^i C_i(\mu) Q_i. \quad (2.1)$$

Here  $Q_i$  are  $\Delta F = 2$  operators,  $G_F$  is the Fermi constant and  $V_{\text{CKM}}$  is the appropriate Cabibbo-Kobayashi-Maskawa (CKM) factor. Because in the GMVF models the CKM matrix is by definition the only source of flavour and CP violation, the Wilson coefficients  $C_i(\mu)$  are *real*. Using this Hamiltonian with the Wilson coefficients evaluated at the appropriate scale  $\mu$  one can calculate  $\Delta F = 2$  amplitudes, in particular the mass differences  $\Delta M_{d,s}$  and the CP violation parameter  $\varepsilon$  measured in  $K \rightarrow \pi\pi$  decays.

The full set of dimension six operators contributing to  $\Delta F = 2$  transitions consists of 8 operators. According to the chirality of the quark fields they can be split into 5 separate sectors. The operators belonging to the VLL, LR and SLL sectors read:

$$\begin{aligned} Q_1^{\text{VLL}} &= (\bar{d}_J \gamma_\mu P_L d_I) (\bar{d}_J \gamma^\mu P_L d_I), \\ Q_1^{\text{LR}} &= (\bar{d}_J \gamma_\mu P_L d_I) (\bar{d}_J \gamma^\mu P_R d_I), \\ Q_2^{\text{LR}} &= (\bar{d}_J P_L d_I) (\bar{d}_J P_R d_I), \\ Q_1^{\text{SLL}} &= (\bar{d}_J P_L d_I) (\bar{d}_J P_L d_I), \\ Q_2^{\text{SLL}} &= (\bar{d}_J \sigma_{\mu\nu} P_L d_I) (\bar{d}_J \sigma^{\mu\nu} P_L d_I), \end{aligned} \quad (2.2)$$

where  $I, J$  are the flavour indices (i.e.  $d_3 \equiv b$ ,  $d_2 \equiv s$ ,  $d_1 \equiv d$  and, analogously,  $u_3 \equiv t$ ,  $u_2 \equiv c$ ,  $u_1 \equiv u$ ),  $\sigma_{\mu\nu} = \frac{1}{2}[\gamma_\mu, \gamma_\nu]$ ,  $P_{L,R} = \frac{1}{2}(1 \mp \gamma_5)$  and the colour indices are contracted

within the brackets. The operators belonging to the VRR and SRR sectors are obtained from  $Q_1^{\text{VLL}}$  and  $Q_i^{\text{SLL}}$  by interchanging  $P_L$  and  $P_R$ . Since QCD preserves chirality, there is no mixing between different sectors. Moreover, the QCD evolution factors from high energy to low energy scales in the VRR and SRR sectors are the same as in the VLL and SLL sectors, respectively. However, one should remember that the initial conditions  $C_i(\mu_t)$  (where  $\mu_t = \mathcal{O}(m_t)$ ) are in general different for operators involving  $P_L$  and  $P_R$ . In the limit in which the effective Hamiltonian (2.1) is dominated by the single  $Q_1^{\text{VLL}}$  operator one recovers the results of the MFV models.

The QCD renormalization group factors relevant for the Hamiltonian (2.1) have been calculated at the NLO level in [27, 28, 29, 30, 31, 32] where the last four papers deal with the LR and SLL(SRR) operators. In particular in ref. [32] master formulae for  $\Delta F = 2$  NLO QCD factors relating  $C_i(\mu_t)$  to  $C_i(\mu)$  where  $\mu_t = \mathcal{O}(m_t)$  and  $\mu = \mathcal{O}(m_b)$  or  $\mu = \mathcal{O}(2 \text{ GeV})$  have been presented and evaluated numerically in the NDR renormalization scheme. Below we will exploit the general formulae of ref. [32] expressing  $\Delta M_d$ ,  $\Delta M_s$  and  $\varepsilon$  in terms of the non-perturbative parameters  $B_i$ .

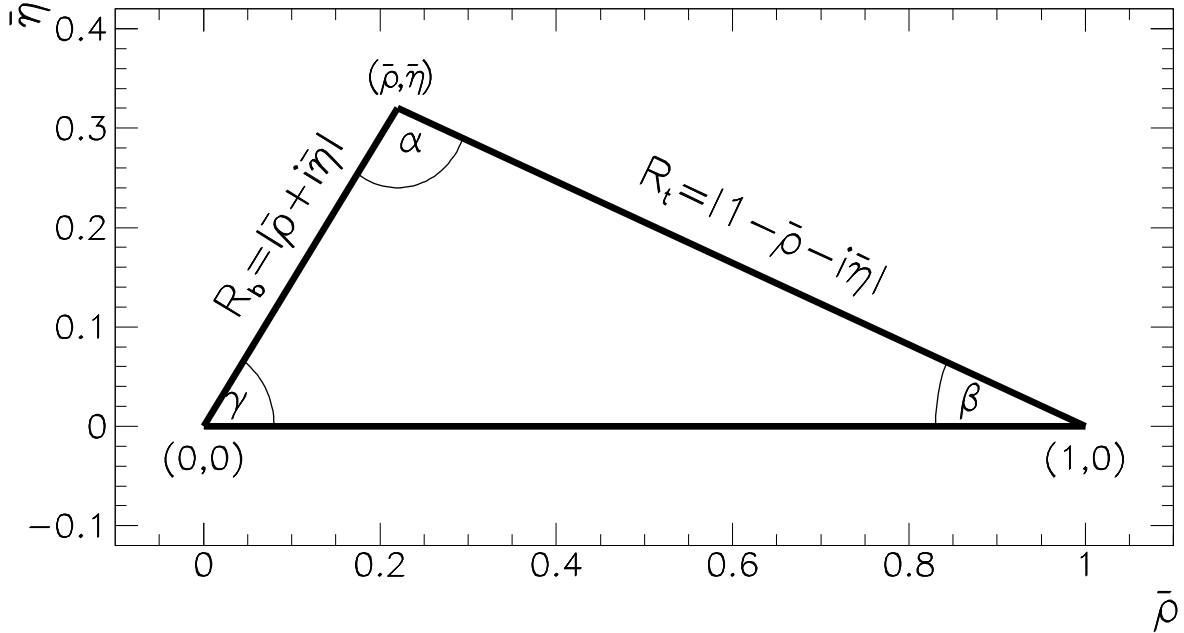


Figure 1: Unitarity Triangle.

## 2.2 $\Delta M_d$ , $\Delta M_s$ , $\varepsilon$ and $\sin 2\beta$ in the GMVF Models

It is straightforward to generalize the formulae of refs. [1, 10, 9, 23] to the case of GMVF models. To this end, following the notation of ref. [7], we introduce three real functions

$$F_{tt}^d = S_0(x_t)[1 + f_d] , \quad F_{tt}^s = S_0(x_t)[1 + f_s] , \quad F_{tt}^\varepsilon = S_0(x_t)[1 + f_\varepsilon] , \quad (2.3)$$

relevant for  $\Delta M_d$ ,  $\Delta M_s$  and  $\varepsilon$  respectively.  $S_0(x_t)$  with  $x_t = m_t^2/M_W^2$  is the function resulting from box diagrams with  $(t, W^\pm)$  exchanges.  $S_0(x_t) \approx 2.38 \pm 0.11$  for  $\bar{m}_t(m_t) = (166 \pm 5)$  GeV. In order not to complicate the expressions below we assume  $F_{tt}^i > 0$ . Generalization to negative  $F_{tt}^i$  can be easily done following the discussion of ref. [23]. We further split the parameters  $f_i$  into universal and non-universal parts

$$f_i = f_{\text{uni}} + \tilde{f}_i \quad (2.4)$$

where  $\tilde{f}_i = 0$  in the MFV models [10]. We have then,

$$\Delta M_q = \frac{G_F^2 M_W^2}{6\pi^2} M_{B_q} \eta_B \hat{B}_{B_q} F_{B_q}^2 |V_{tq}|^2 F_{tt}^q, \quad q = d, s \quad (2.5)$$

where  $F_{B_q}$  is the  $B_q$ -meson decay constant,  $\hat{B}_{B_q}$  is a non-perturbative parameter and  $\eta_B = 0.55$  is the QCD factor [27, 28]. The measurements of  $\Delta M_q$  determine the length  $R_t$  of one side of the unitarity triangle (shown in fig. 1) defined by

$$R_t \equiv \frac{|V_{td} V_{tb}^*|}{|V_{cd} V_{cb}^*|} = \sqrt{(1 - \bar{\varrho})^2 + \bar{\eta}^2} = \frac{1}{\lambda} \left| \frac{V_{td}}{V_{cb}} \right| . \quad (2.6)$$

Here  $\bar{\varrho} = \varrho(1 - \lambda^2/2)$ ,  $\bar{\eta} = \eta(1 - \lambda^2/2)$  [8], and  $\lambda$ ,  $\varrho$  and  $\eta$  are the Wolfenstein parameters [33]. As in ref. [23] we set  $\lambda = 0.222$  in the analytic formulae below.\* Other input parameters are collected in table 1.

From  $\Delta M_d$  and  $\Delta M_d/\Delta M_s$  we find

$$R_t = 1.084 \frac{R_0}{A} \frac{1}{\sqrt{F_{tt}^d}}, \quad R_0 \equiv \sqrt{\frac{\Delta M_d}{0.487/\text{ps}}} \left[ \frac{230 \text{ MeV}}{\sqrt{\hat{B}_{B_d}} F_{B_d}} \right] \sqrt{\frac{0.55}{\eta_B}} \quad (2.7)$$

and

$$R_t = 0.819 \xi \sqrt{\frac{\Delta M_d}{0.487/\text{ps}}} \sqrt{\frac{15/\text{ps}}{\Delta M_s}} \sqrt{R_{sd}} , \quad (2.8)$$

\*Because of that some numerical factors in the formulae below differ from their counterparts in refs. [1, 10] where  $\lambda = 0.220$  has been used. This change has only a very small impact on the numerical analysis. In particular the bound (1.6) remains unchanged. On the other hand the increased value of  $\lambda$  shifts  $V_{ud}$  closer to its experimental value. See ref. [11] for the discussion of this point.

Table 1: The ranges of the input parameters.

Quantity	Central value	Error
$\lambda$	0.222	$\pm 0.0018$
$ V_{cb} $	0.041	$\pm 0.002$
$ V_{ub}/V_{cb} $	0.085	$\pm 0.018$
$ V_{ub} $	0.00349	$\pm 0.00076$
$\hat{B}_K$	0.85	$\pm 0.15$
$\varepsilon$	$2.280 \times 10^{-3}$	$\pm 0.013 \times 10^{-3}$
$\sqrt{\hat{B}_{B_d}} F_{B_d}$	230 MeV	$\pm 40$ MeV
$\sqrt{\hat{B}_{B_s}} F_{B_s}$	265 MeV	$\pm 40$ MeV
$\xi$	1.15	$\pm 0.06$
$m_t$	166 GeV	$\pm 5$ GeV
$\Delta M_d$	0.487/ps	$\pm 0.009$ /ps
$\Delta M_s$	$> 15.0$ /ps	
$M_W$	80.4 GeV	

respectively where the Wolfenstein parameter  $A$  is defined by  $|V_{cb}| = A\lambda^2$ . Here

$$R_{sd} = \frac{1 + f_s}{1 + f_d}, \quad \xi = \frac{F_{B_s} \sqrt{\hat{B}_{B_s}}}{F_{B_d} \sqrt{\hat{B}_{B_d}}}. \quad (2.9)$$

The measurement of the parameter  $\varepsilon$  imposes the constraint which reads:

$$\bar{\eta} \left[ (1 - \bar{\varrho}) A^2 \eta_2 F_{tt}^\varepsilon + P_c(\varepsilon) \right] A^2 \hat{B}_K = 0.204, \quad (2.10)$$

where  $\eta_2 = 0.57$  is the QCD factor [27] and  $P_c(\varepsilon)$  summarizes the contributions not proportional to  $V_{ts}^* V_{td}$ . With (2.7) and (2.10), the formula of ref. [10] for  $\sin 2\beta$  valid in MFV models generalizes to

$$\sin 2\beta = \frac{1.65}{R_0^2 \eta_2} R_{d\varepsilon} \left[ \frac{0.204}{A^2 \hat{B}_K} - \bar{\eta} P_c(\varepsilon) \right], \quad R_{d\varepsilon} = \frac{1 + f_d}{1 + f_\varepsilon}. \quad (2.11)$$

Note that new physics can affect  $\sin 2\beta$  both through  $f_d$  and  $f_\varepsilon$  in (2.11) and indirectly through  $\bar{\eta}$ . We assume as in [9, 10] that new physics contributions to  $P_c(\varepsilon)$  are negligible. In this case  $P_c(\varepsilon) = 0.30 \pm 0.05$  [34].

## 2.3 How to distinguish GMFV from MFV

In general, the presence of new  $\Delta F = 2$  operators causes the departure from the relation  $F_{tt}^d = F_{tt}^s = F_{tt}^\varepsilon$  valid in the MFV models. This means for instance that the ratio  $\Delta M_s/\Delta M_d$ , being now dependent on new physics contributions, cannot be used any longer for the construction of the universal unitarity triangle [9]. In other words the dictionary between  $R_t$  and  $\Delta M_s/\Delta M_d$ , as given by (2.8), differs from the corresponding one in the MFV models because  $R_{sd} \neq 1$ . This fact offers a possibility to distinguish experimentally between these two classes of models. Two strategies are presented below. Because of the unitarity of the CKM matrix these strategies are related to each other.

### 2.3.1 Strategy A

For given values of  $|V_{ub}/V_{cb}|$  and  $\Delta M_s/\Delta M_d$  one can determine (see fig. 1)

$$R_b \equiv \frac{|V_{ud}V_{ub}^*|}{|V_{cd}V_{cb}^*|} = \sqrt{\bar{\varrho}^2 + \bar{\eta}^2} = (1 - \frac{\lambda^2}{2}) \frac{1}{\lambda} \left| \frac{V_{ub}}{V_{cb}} \right|, \quad (2.12)$$

and  $R_t$  by means of (2.8), respectively. This gives the apex of the unitarity triangle with

$$\bar{\varrho} = \frac{1}{2}(1 + R_b^2 - R_t^2), \quad \bar{\eta} = \sqrt{R_b^2 - \bar{\varrho}^2}. \quad (2.13)$$

and consequently

$$\sin 2\beta = \frac{2\bar{\eta}(1 - \bar{\varrho})}{R_t^2}. \quad (2.14)$$

These formulae establish the relation between  $\sin 2\beta$  and  $\Delta M_s/\Delta M_d$  that depends on the ratio  $R_{sd}$ . In fig. 2 we show  $\sin 2\beta$  as a function of  $\Delta M_s/\Delta M_d$  for  $|V_{ub}/V_{cb}| = 0.070, 0.085, 0.10$  and different values of the ratio  $R_{sd}$ . To this end we have set  $\xi = 1.15$ . We observe that for  $\Delta M_s/\Delta M_d$  below 40 the distinction between GMFV and MFV models will be difficult unless the values of  $\xi$ ,  $|V_{ub}/V_{cb}|$ ,  $a_{\psi K_S}$  and  $\Delta M_s$  will be known very accurately or the value of  $R_{sd}$  differs substantially from unity. For larger values of  $\Delta M_s/\Delta M_d$  the distinction is clearer.

From fig. 2 the impact of the measurement of  $\Delta M_s/\Delta M_d$  on the allowed values of  $\sin 2\beta$  is clearly seen. For  $0.8 < R_{sd} < 1.2$  and  $\Delta M_s/\Delta M_d < 40$  only values compatible with current experimental result (1.3) and well above the bound (1.6) are allowed. On the other hand, for sufficiently low or sufficiently large values of  $R_{sd}$ , smaller values of  $\sin 2\beta$  are also possible. While such low values of  $\sin 2\beta$  are still compatible with the BaBar result, they seem to be excluded by the Belle measurement of  $a_{\psi K_S}$ . In fact, as follows from fig. 2, the latter measurement can be accommodated only if  $R_{sd} \approx 1$  and  $|V_{ub}/V_{cb}| \approx 0.1$ .

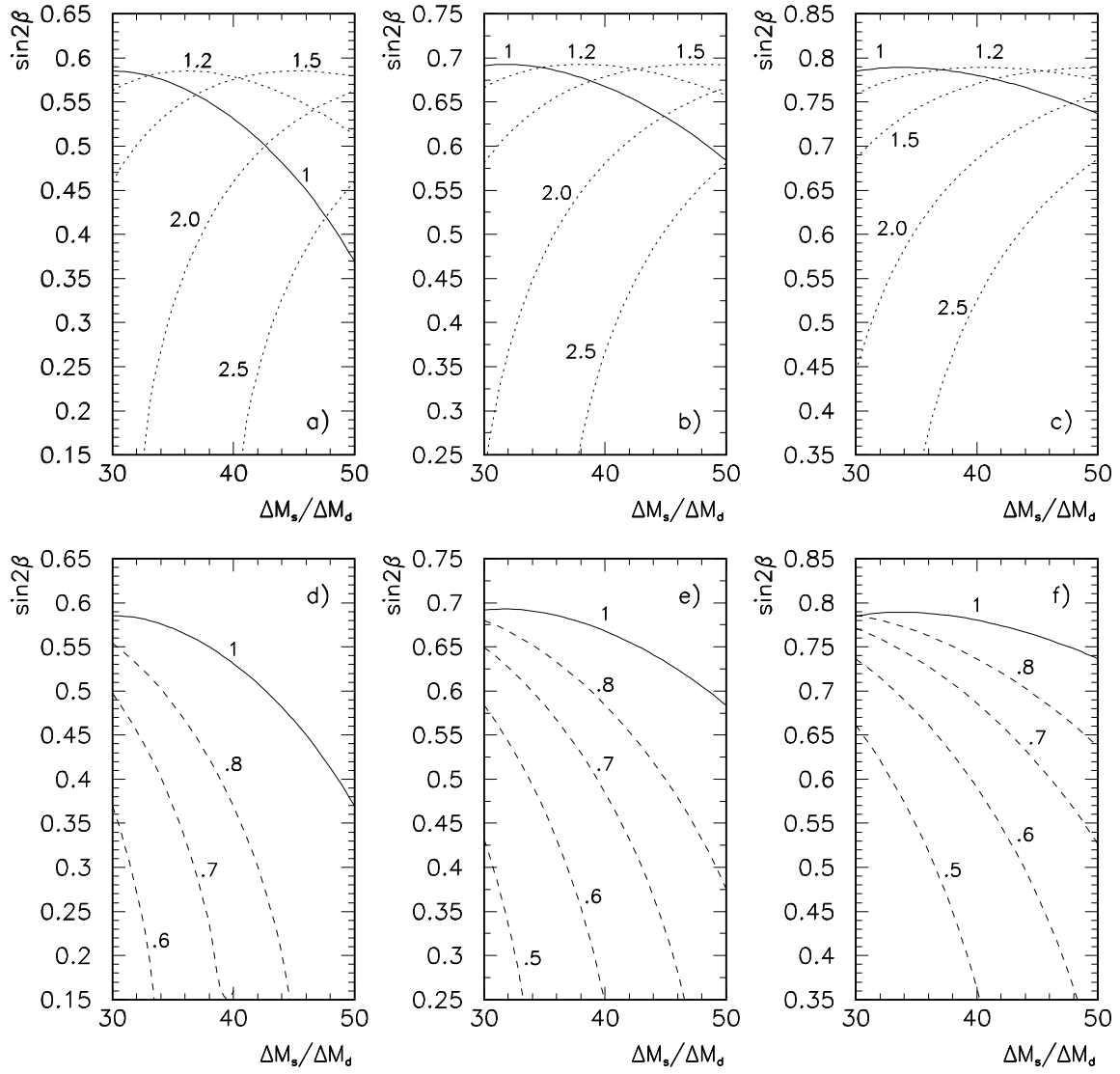


Figure 2:  $\sin 2\beta$  as a function of  $\Delta M_s/\Delta M_d$  for  $|V_{ub}/V_{cb}| = 0.070$  (panels a and d), 0.085 (panels b and e), and 0.10 (panels c and f) for different values of  $R_{sd}$  (marked on the curves) and  $\xi = 1.15$ .

It is also easy to find that the two possibilities, small  $R_{sd}$  and large  $R_{sd}$ , favour small and large values of the angle  $\gamma$  in the unitarity triangle, respectively. Which of these two possibilities is favoured by the data can only be decided by other measurements. This includes  $\varepsilon$ ,  $\Delta M_d$  alone and in particular a direct measurement of  $\gamma$ . This brings us to the second strategy.

### 2.3.2 Strategy B

The angle  $\gamma$  in the unitarity triangle can be found from  $R_t$  and  $\beta$  determined through (1.1) by using the relation

$$\cot \gamma = \frac{1 - R_t \cos \beta}{R_t \sin \beta}. \quad (2.15)$$

Expressing  $R_t$  in terms of  $\Delta M_s/\Delta M_d$  by means of (2.8) allows to calculate  $\gamma$  as a function of  $\sin 2\beta$ ,  $\Delta M_s/\Delta M_d$  and  $R_{sd}$ . For  $R_{sd} \neq 1$  the predictions for  $\gamma$  in GMFV models will generally differ from those in the MFV models. Comparing these predictions with future direct measurements of  $\gamma$  it will be possible to distinguish between these two classes of models and check whether the inclusion of new operators is required by the data. In fig. 3 we show  $\gamma$  as a function of  $\Delta M_s/\Delta M_d$  for  $\sin 2\beta = 0.4, 0.6, 0.8$  and various values of  $R_{sd}$ .

We observe that the distinction between MFV and GMFV models in this strategy is, in contrast to strategy A, very transparent in the full range of  $\Delta M_s/\Delta M_d$  considered. As this strategy involves only  $a_{\psi K_S}$  and  $\Delta M_s/\Delta M_d$ , that are theoretically cleaner than  $|V_{ub}/V_{cb}|$ , it is this strategy which in the future should play the crucial role in the distinction between the MFV and GMFV models. The ratio  $\Delta M_s/\Delta M_d$  and the asymmetry  $a_{\psi K_S}$  should be determined very precisely in the coming years. The determination of  $\gamma$  is more difficult but should be achieved at LHCb and BTeV. Some information on the angle  $\gamma$  should also be gained from the  $B_d \rightarrow \pi K$  decays measured by CLEO, BaBar and Belle and by the combination of  $B_d \rightarrow \pi^+ \pi^-$  rate (already measured by these three collaborations) and the rate of the  $B_s \rightarrow K^+ K^-$  decay [35] which are going to be measured at Tevatron.

As seen in fig. 3 the values of  $\gamma$  for  $R_{sd} \leq 1.2$  are below  $90^\circ$ . On the other hand for substantially higher  $R_{sd}$  also  $\gamma > 90^\circ$  is possible. The possibility of  $\gamma > 90^\circ$  resulting from the unitarity triangle fits is very interesting in view of several analyses [36, 37, 38, 39] of two-body non-leptonic decays  $B \rightarrow \pi K, \pi\pi$  that favour  $\gamma > 90^\circ$  in contradiction with the usual unitarity triangle analyses that confidently give  $\gamma < 90^\circ$ . With increasing  $\Delta M_s/\Delta M_d$  this problem will become more serious.

In view of sizable theoretical uncertainties in the analyses of  $B \rightarrow \pi K, \pi\pi$  and of large experimental errors in the corresponding branching ratios it is not yet clear whether the discrepancy in question is serious. For instance [40] sizable contributions of the so-called charming penguins to the  $B \rightarrow \pi K$  amplitudes could shift  $\gamma$  extracted from these decays below  $90^\circ$  but at present these contributions cannot be calculated reliably. Similar role could be played by annihilation contributions and large non-factorizable  $SU(3)$  breaking effects [36]. Also, a new physics contribution in the electroweak penguin sector could also shift  $\gamma$  to the first quadrant [36]. It should be however emphasized that the problem with the angle  $\gamma$ , if it persisted, would put into difficulties not only the SM but also the full

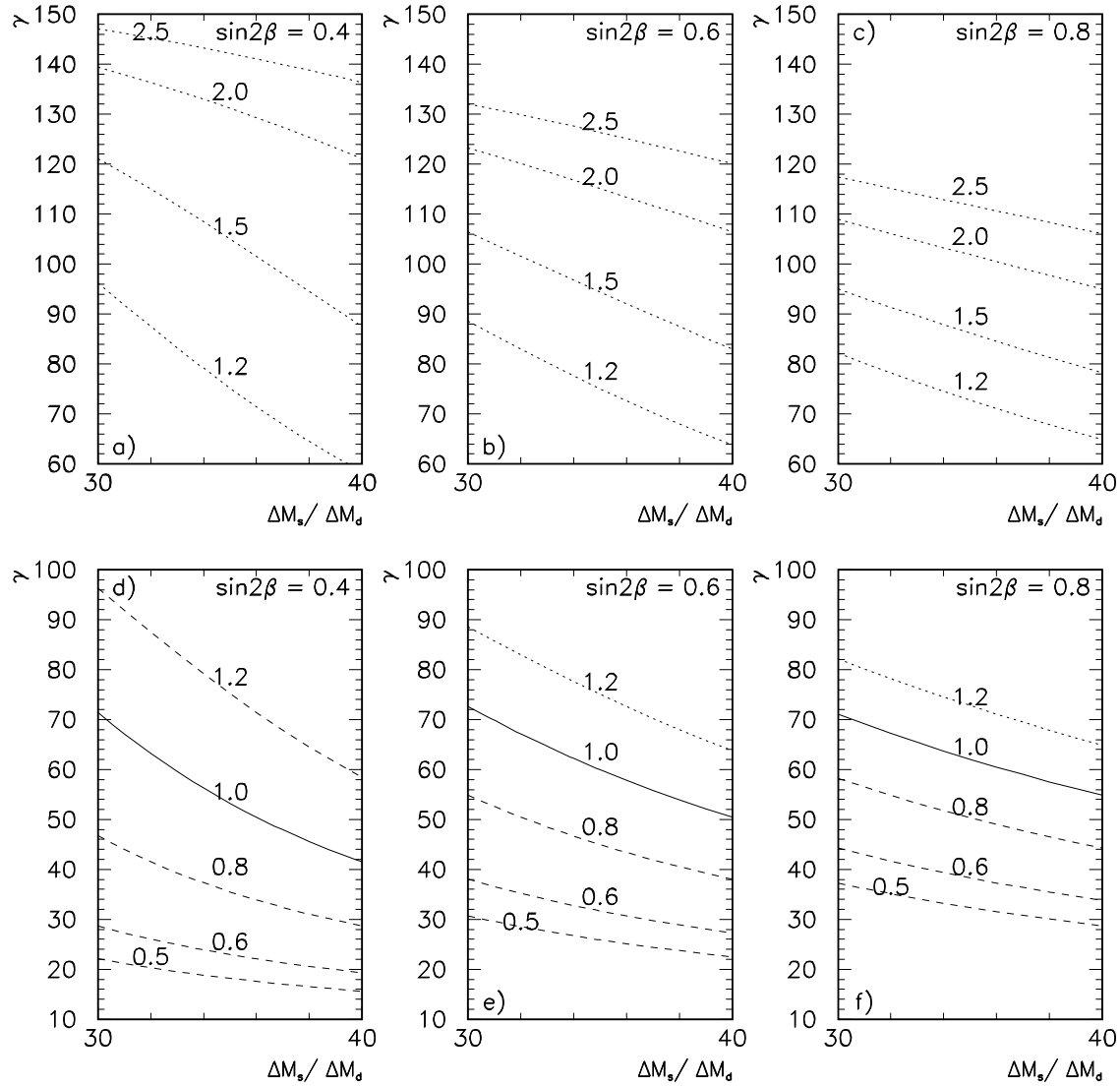


Figure 3:  $\gamma$  as a function of  $\Delta M_s/\Delta M_d$  for  $\sin 2\beta = 0.4, 0.6, 0.8$  and various values of  $R_{sd}$  (marked on the curves).

class of MFV models in which the lower bound on  $\Delta M_s/\Delta M_d$  implies  $\gamma < 90^\circ$ . On the other hand as seen in fig. 3 for sufficiently high values of  $R_{sd}$ , the angle  $\gamma$  resulting from the unitarity triangle analysis can easily be in the second quadrant provided  $\Delta M_s/\Delta M_d$  is not too large.

Clearly a general analysis of the unitarity triangle involving  $\varepsilon$ ,  $\Delta M_{s,d}$ ,  $|V_{ub}/V_{cb}|$  and  $|V_{cb}|$  can also be used to search for the effects caused by the new operators but the two strategies outlined above have in our opinion the best chance to distinguish between MFV

and GMFV models in a transparent manner.

### 2.3.3 Unitarity Triangle, $\sin 2\beta$ and $\gamma$

A different version of strategy B is to construct the unitarity triangle by means of the ratio  $\Delta M_s/\Delta M_d$  and the asymmetry  $a_{\psi K_S}$ . With  $R_t$  given by (2.8) the parameters  $\bar{\varrho}$  and  $\bar{\eta}$  can be determined from the formulae<sup>†</sup>

$$\begin{aligned}\bar{\eta} &= \frac{R_t}{2} \left( \sqrt{1 + \sin 2\beta} - \sqrt{1 - \sin 2\beta} \right) \\ \bar{\varrho} &= 1 - \frac{R_t}{2} \left( \sqrt{1 + \sin 2\beta} + \sqrt{1 - \sin 2\beta} \right)\end{aligned}\quad (2.16)$$

(recall that in GMFV models  $\sin 2\beta = a_{\psi K_S}$ ) obtained directly from eqs. (2.6) and (2.14). These formulae are equivalent to those presented in [9, 23] but are more elegant.

As an illustration we show in fig. 4 the ranges of  $(\bar{\varrho}, \bar{\eta})$  allowed by the hypothetical measurement  $\Delta M_s = (18.0 \pm 0.5)/ps$  for three values of  $a_{\psi K_S}$  and different values of  $R_{sd}$ . Solid ellipses correspond to  $R_{sd} = 1$  valid in particular in MFV models. We also show the  $R_b$ -constraint, eq. (2.12), with  $R_b = 0.37 \pm 0.08$  and as a useful reference the  $\varepsilon$ -constraint (2.10) with  $1 + f_\varepsilon = 1$  corresponding to the SM.

From fig. 4 it is clear that for  $a_{\psi K_S} = 0.80 \pm 0.05$  the class of models giving  $R_{sd} = 1$  and  $1 + f_\varepsilon = 1$  (which includes also the MFV models) is consistent with all constraints but only for  $\sin 2\beta$  in the lower part of the chosen range. There is also a room for contributions of new operators resulting in  $R_{sd} \neq 1$  provided  $0.7 \leq R_{sd} \leq 1.4$ . As in strategy B they could be distinguished through the value of the angle  $\gamma$ . We also observe that no sizable contributions to  $\varepsilon$  beyond the SM ones are required. For  $a_{\psi K_S} = 0.60 \pm 0.05$  models giving  $R_{sd} = 1$  are consistent with the  $R_b$ - and  $\varepsilon$ -constraints for  $\sin 2\beta$  in the full chosen range. In this scenario models with  $0.8 \leq R_{sd} \leq 2.0$  and no sizable new contributions to  $\varepsilon$  and models with  $R_{sd} < 0.8$  but with  $1 + f_\varepsilon > 1.0$  are favoured. Again the measurement of  $\gamma$  could distinguish between these possibilities. It is interesting to note that for  $1.5 \leq R_{sd} \leq 2.0$  it is possible to have  $\gamma > 90^\circ$  even for  $1 + f_\varepsilon = 1$ . Finally, for  $a_{\psi K_S} = 0.4$  models giving  $R_{sd} = 1$  are ruled out as they do not satisfy the  $R_b$ -constraint. In order to reconcile this constraint with  $a_{\psi K_S} \approx 0.4$ , values of  $R_{sd}$  substantially different from unity are required. Moreover in the case of  $R_{sd} < 1.0$  one has  $\gamma \ll 90^\circ$  but large new contributions to  $\varepsilon$  leading to  $1 + f_\varepsilon > 1.0$  and  $R_{d\varepsilon} < 1.0$  are mandatory. In contrast, if  $R_{sd} \gtrsim 2.0$   $\gamma$  can be much bigger than  $90^\circ$  even without new contributions to  $\varepsilon$  i.e. with  $1 + f_\varepsilon \approx 1$ .

---

<sup>†</sup>This is valid for  $-\pi/4 < \beta < \pi/4$ ; for other ranges of  $\beta$  similar formulae can be obtained.

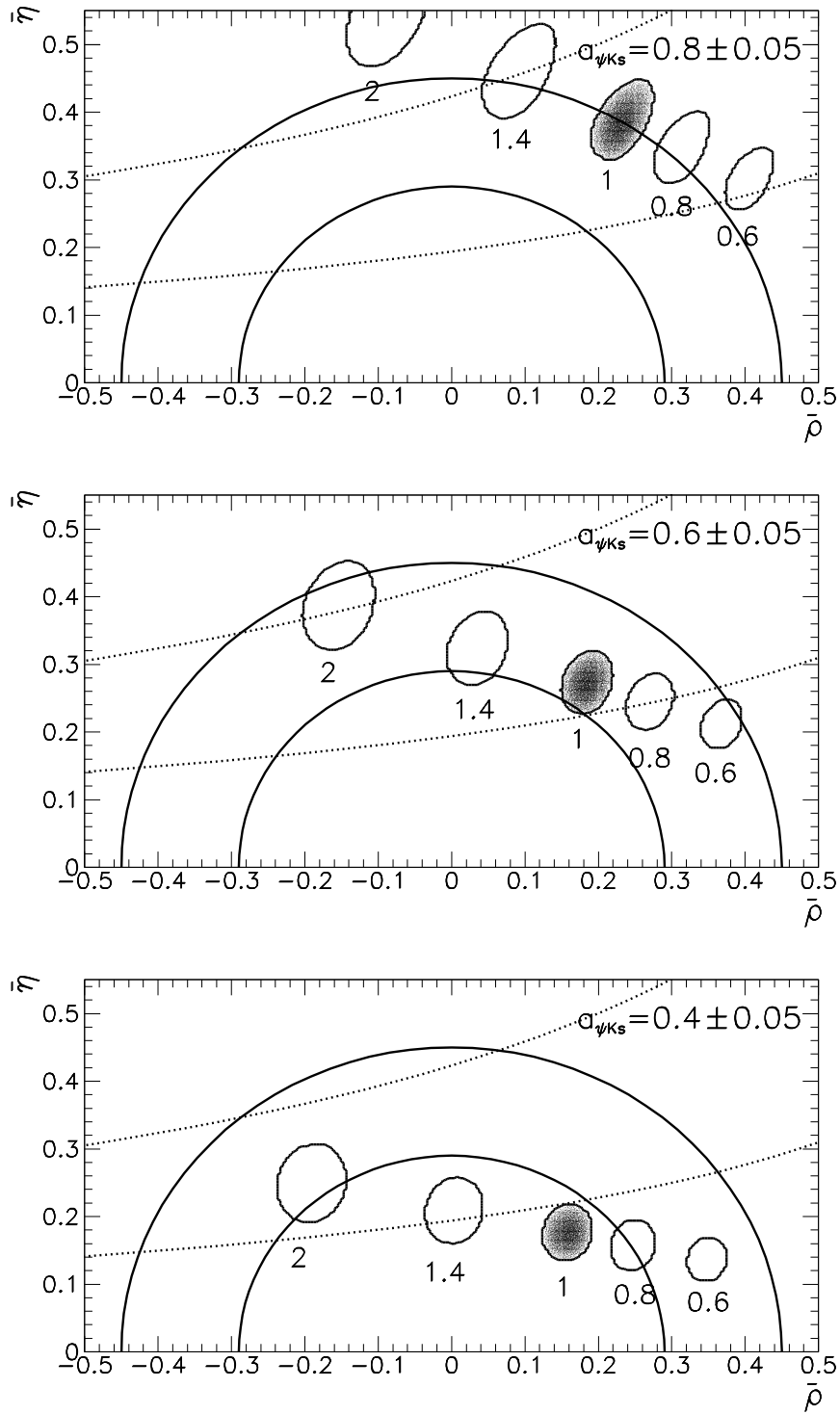


Figure 4: Ranges of  $(\bar{\rho}, \bar{\eta})$  allowed in  $1\sigma$  for  $\Delta M_s = (18.0 \pm 0.5)/ps$ , three values of  $a_{\psi K_S}$  and different values of  $R_{sd}$  (marked in the figures). Black spots correspond to  $R_{sd} = 1$ . Dotted lines show the constraint from the parameter  $\varepsilon$ , eq. (2.10), for  $1 + f_\varepsilon = 1$ .

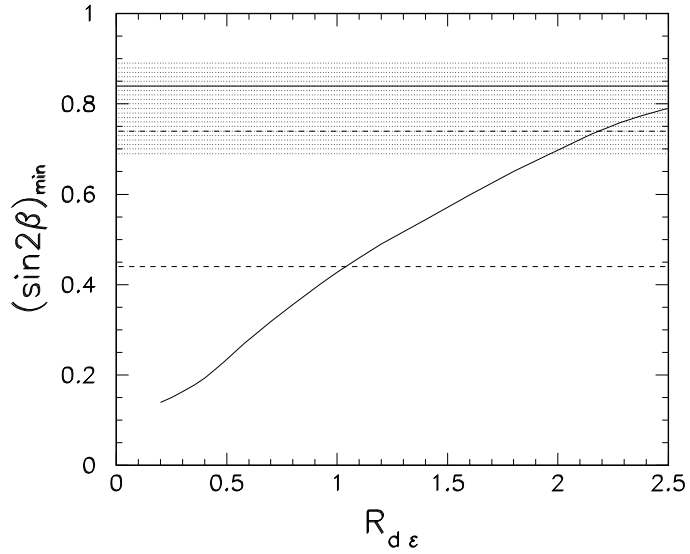


Figure 5: Lower bound on  $\sin 2\beta$  in GMFV models as a function of the ratio  $R_{d\epsilon}$ . Dashed lines show the 1-sigma BaBar result ( $\sin 2\beta = 0.59 \pm 0.15$ ), the horizontal solid line shows the lower limit from the Belle measurement ( $\sin 2\beta = 0.99 \pm 0.15$ ) and the shaded area corresponds to the  $\sin 2\beta$  range presently allowed in GMFV models at  $1\sigma$  by the official grand average (1.3).

As in some scenarios discussed above  $R_{d\epsilon}$  must differ from unity, we show in fig. 5 the dependence of the lower bound for  $\sin 2\beta$  on the value of  $R_{d\epsilon}$  together with the  $1\sigma$  BaBar result and the present official experimental  $1\sigma$  band (1.3) for  $a_{\psi K_S} = \sin 2\beta$ . It follows, that at present the ratio  $R_{d\epsilon}$  would be constrained at  $1\sigma$  by the BaBar result to be less than 2.2 but the analogous limit following from the grand average (1.3) is much higher. Fig. 5 has been obtained for  $R_{sd} = 1.0$  but  $(\sin 2\beta)_{\min}$  depends only very weakly on the ratio  $R_{sd}$ : very similar curves are obtained also for  $0.6 \leq R_{sd} \leq 2.0$ .

## 2.4 Constraints on GMFV models from unitarity triangle

In the preceding subsection we have presented two strategies which in principle should allow to decide on the basis of experimental measurements whether going beyond the MFV models is necessary, i.e. to establish whether  $R_{sd} \neq 1$ . In this section we want to explore constraints and correlations imposed by the experimental data (present and future) and the unitarity of the CKM matrix on the functions  $F_{tt}^i$ . These constraints can be then effectively used to test the specific GMFV models of new physics.

The first constraint follows from fitting the formula (2.5) to the measured (in the near

future) value of  $\Delta M_s$ . This determines  $1 + f_s$  (or  $F_{tt}^s$ ):

$$1 + f_s = 0.80 \left[ \frac{2.38}{S_0(x_t)} \right] \left[ \frac{265 \text{ MeV}}{\sqrt{\hat{B}_{B_s}} F_{B_s}} \right]^2 \left[ \frac{0.55}{\eta_B} \right] \left[ \frac{0.041}{|V_{ts}|} \right]^2 \left[ \frac{\Delta M_s}{15/\text{ps}} \right] \quad (2.17)$$

This formula follows also by equating  $R_t$  determined from  $\Delta M_d$  alone (eq. (2.7)) and  $R_t$  determined from the ratio  $\Delta M_s/\Delta M_d$  (eq. (2.8)). Scanning over uncertainties in the ranges specified in table 1 and setting  $|V_{ts}| = |V_{cb}|$  gives

$$0.52 \left[ \frac{\Delta M_s}{15/\text{ps}} \right] < 1 + f_s < 1.29 \left[ \frac{\Delta M_s}{15/\text{ps}} \right] \quad (2.18)$$

(At present this gives of course  $1 + f_s > 0.52$ .) It is worth emphasizing that this bound is independent of the uncertainties of  $|V_{ub}/V_{cb}|$  as well as of any assumptions about possible new physics contribution in the  $\bar{K}^0-K^0$  system. Therefore the GMFV models not respecting it are (will be) ruled out. We will see in sec. 4.2 that the MSSM, for some values of its parameters, violates precisely this bound.

Next, there are bounds on  $R_t$  coming from the requirement that

$$1 - R_b < R_t < 1 + R_b \quad (2.19)$$

which gives  $0.54 < R_t < 1.46$ . This can be used to constrain either  $1 + f_d$  or  $R_{sd}$  depending on how one determines  $R_t$ . In the first case one gets

$$0.20 < 1 + f_d < 4.24 \quad (2.20)$$

and in the second

$$0.29 \left[ \frac{\Delta M_s}{15/\text{ps}} \right] < R_{sd} < 2.73 \left[ \frac{\Delta M_s}{15/\text{ps}} \right]. \quad (2.21)$$

More stringent constraint on  $R_{sd}$  (if  $R_t$  is determined from (2.8)) or  $1 + f_d$  (if  $R_t$  is determined from (2.7)) will follow from  $R_b$  combined with the information about  $\sin 2\beta$  obtained from future accurate measurements of the asymmetry  $a_{\psi K_S}$ . It is easy to see that for  $\sin 2\beta \lesssim 0.34$  there are two allowed bands of  $1 + f_d$  corresponding to two possible solutions<sup>‡</sup> for  $R_t$ :

$$R_t = \cos \beta \mp \sqrt{R_b^2 - \sin^2 \beta} \quad (2.22)$$

(the solutions with  $- (+)$  correspond to smaller (larger) values of the angle  $\gamma$ ). For larger values of  $\sin 2\beta$  the two bands overlap which means that there is only one allowed range of

---

<sup>‡</sup>The band of allowed  $R_t$  values splits into two for  $\sin 2\beta \approx 0.56$  corresponding to  $\sin \beta = R_b^{\min}$ . Additional uncertainties in translating  $R_t$  into  $1 + f_d$  (or  $R_{sd}$ ) result in lowering the value of  $\sin 2\beta$  below which the two allowed bands of  $1 + f_d$  (or  $R_{sd}$ ) appear.

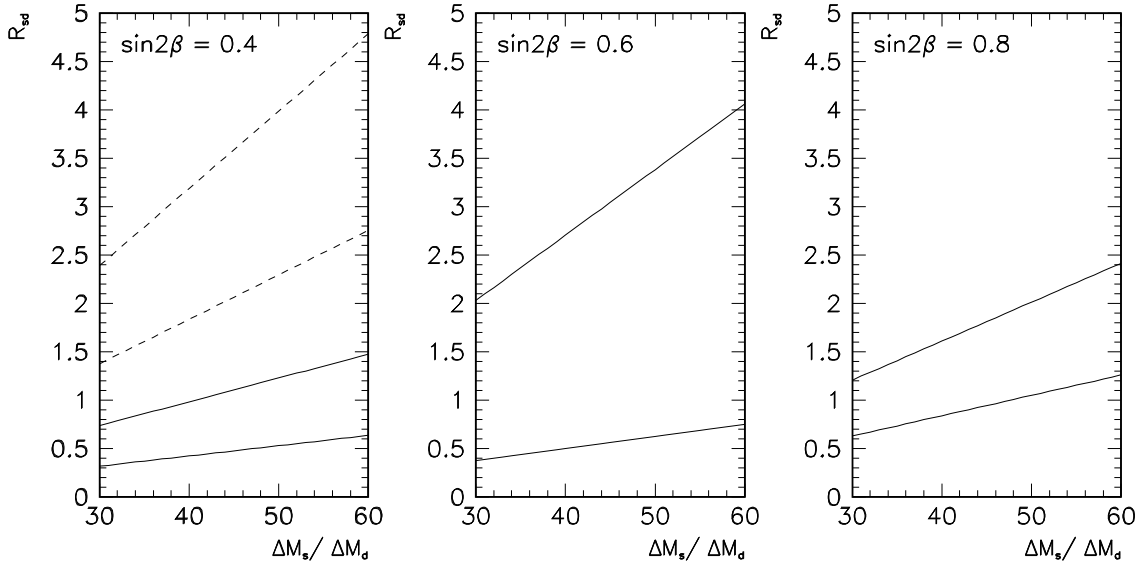


Figure 6: Allowed bands of  $R_{sd}$  as a function of  $\Delta M_s/\Delta M_d$  for different values of  $\sin 2\beta$ .

$1 + f_d$  (or  $R_{sd}$ ). For example scanning over uncertainties one obtains:  $0.21 < 1 + f_d < 0.78$  or  $0.84 < 1 + f_d < 4.15$  for  $\sin 2\beta = 0.2$ ,  $0.23 < 1 + f_d < 3.85$  for  $\sin 2\beta = 0.4$ ,  $0.26 < 1 + f_d < 3.27$  for  $\sin 2\beta = 0.6$  and  $0.44 < 1 + f_d < 1.98$  for  $\sin 2\beta = 0.8$ . The corresponding allowed ranges of  $R_{sd}$  are shown in fig. 6 for different values of  $\sin 2\beta$  as functions of the measured values of  $\Delta M_s/\Delta M_d$ .

Further constraints correlating  $1 + f_\varepsilon$  with  $1 + f_d$  can be obtained by using the experimental information about the parameter  $\varepsilon$ . To this end, with a range of  $R_t$  determined from  $1 + f_d$  and  $\Delta M_d$  by scanning over the relevant uncertainties, one checks whether there exist values of  $\bar{\rho}$  and  $\bar{\eta}$  satisfying eqs. (2.6) and (2.10) for a given value of  $1 + f_\varepsilon$ . It is easy to see that from  $\Delta M_d$  and  $\varepsilon$  alone only a very weak lower bound on  $|1 + f_\varepsilon|$  can exist for  $1 + f_d \gtrsim 1.8$ . As a next step, one can impose the constraint from  $R_b$  (eq. (2.12)). The resulting allowed range in the plane  $(1 + f_d, 1 + f_\varepsilon)$  is shown in fig. 7a,b by the dashed lines (their vertical parts correspond to the lower bound (2.20)). For  $1 + f_d$  in the range (2.20) no upper limit on  $|1 + f_\varepsilon|$  from  $\Delta M_d$ ,  $\varepsilon$  and  $R_b$  exists (except for a very narrow range  $0.7 < 1 + f_d < 0.85$ ). This is because for almost all values of  $1 + f_d$  satisfying (2.20) the range of possible values of  $R_t$  is such that it is possible to satisfy the constraint from  $R_b$  with  $\bar{\eta} = 0$  which in turn allows to suppress arbitrarily large values of  $|1 + f_\varepsilon|$  and to satisfy the eq. (2.10).

It is also interesting to assume that the asymmetry  $a_{\psi K_S}$  (i.e.  $\sin 2\beta$  in GMFV models)

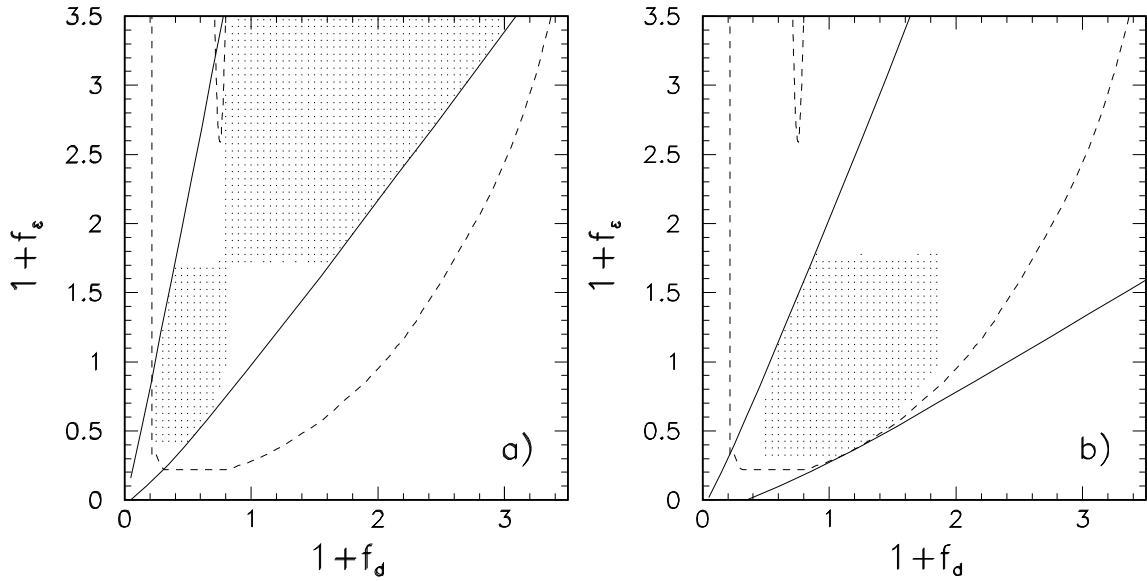


Figure 7: Allowed ranges of  $1+f_d$  and  $1+f_\varepsilon$ .  $\Delta M_d$ ,  $\varepsilon$  and  $R_b$  allow the region delimited by the dashed lines. Regions between the solid lines are allowed by  $\Delta M_d$ ,  $\varepsilon$  and  $\sin 2\beta = 0.4$  (panel a) and  $\sin 2\beta = 0.8$  (panel b). Dotted regions are allowed by  $\Delta M_d$ ,  $\varepsilon$  and  $R_b$  for  $\sin 2\beta = 0.4$  and  $0.8$  in panels a) and b), respectively.

is measured with sufficient accuracy and to correlate  $1+f_\varepsilon$  with  $1+f_d$  by using the experimental information about  $\Delta M_d$  and  $\varepsilon$  for fixed values of  $\sin 2\beta$ . To this end, for  $R_t$  given by eq. (2.7) one determines the parameters  $\bar{\rho}$  and  $\bar{\eta}$  from the formulae (2.16) and checks whether eq. (2.10) can be satisfied. Constraints on the plane  $(1+f_d, 1+f_\varepsilon)$  obtained in this way are shown in fig. 7a for  $\sin 2\beta = 0.4$  and in fig. 7b for  $\sin 2\beta = 0.8$  by the solid lines. It should be stressed that it is the constraint from the  $a_{\psi K_S}$  asymmetry which eliminates solutions with  $\bar{\eta} \approx 0$  thus providing, for fixed  $1+f_d$ , the upper bound on  $1+f_\varepsilon$ . In agreement with the bound (1.6) we observe that for  $\sin 2\beta = 0.4$ ,  $R_{d\varepsilon} \equiv (1+f_d)/(1+f_\varepsilon)$  has to deviate from unity while for  $\sin 2\beta = 0.8$  points corresponding to  $R_{d\varepsilon} = 1$  lie within the allowed region.

Finally, one can impose also the constraints from  $R_b$  (2.12). The allowed ranges in the  $(1+f_d, 1+f_\varepsilon)$  planes are dotted in figs. 7a,b. They are not simply given by the intersection of the regions allowed respectively by  $(\Delta M_d, \varepsilon, R_b)$  and  $(\Delta M_d, \varepsilon, \sin 2\beta)$  because the same point in the  $(1+f_d, 1+f_\varepsilon)$  plane may require different  $\bar{\rho}$  and  $\bar{\eta}$  to be compatible with the two above sets of experimental data.

For a fixed value of the ratio  $\Delta M_s/\Delta M_d$  the same analysis can be also repeated for the  $(R_{sd}, 1+f_\varepsilon)$  plane. However, since the value of  $\Delta M_s/\Delta M_d$  serves only to determine  $R_t$  from eq. (2.8) we show instead in fig. 8 the allowed ranges in the plane  $(\kappa R_{sd}, 1+f_\varepsilon)$  where

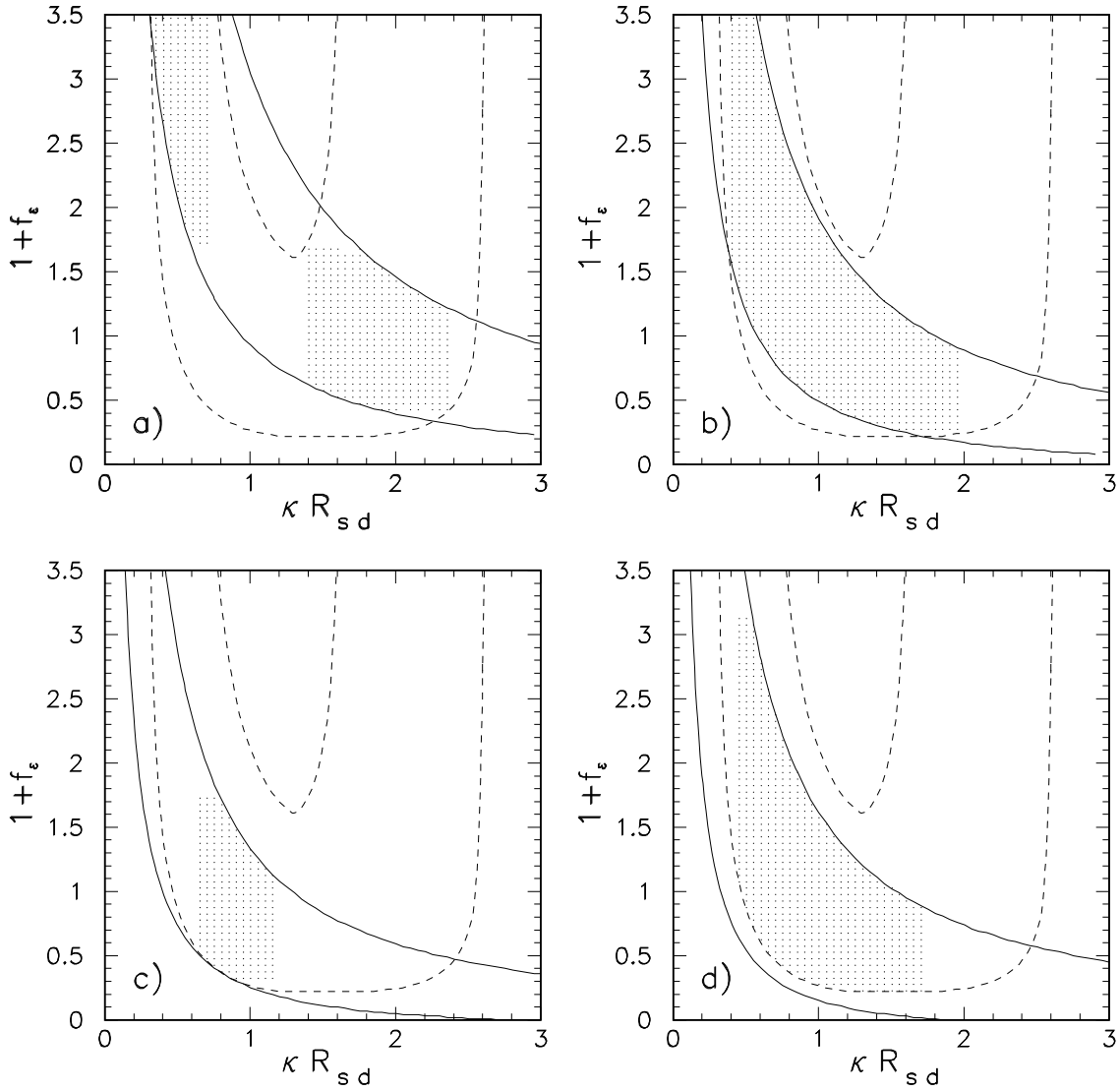


Figure 8: Allowed ranges of  $\kappa R_{sd}$  and  $1 + f_\varepsilon$  where  $\kappa \equiv \frac{30}{\Delta M_s/\Delta M_d}$ .  $\Delta M_s/\Delta M_d$ ,  $\varepsilon$  and  $R_b$  allow the region delimited by the dashed lines. Regions between the solid lines are allowed by  $\Delta M_s/\Delta M_d$ ,  $\varepsilon$  and  $\sin 2\beta = 0.4$  (panel a),  $\sin 2\beta = 0.6$  (panel b),  $\sin 2\beta = 0.8$  (panel c) and  $\sin 2\beta = 0.79 \pm 10$  (panel d). Dotted regions are allowed by  $\Delta M_s/\Delta M_d$ ,  $\varepsilon$ ,  $R_b$  and the corresponding value of  $\sin 2\beta$ .

$\kappa \equiv \frac{30}{\Delta M_s/\Delta M_d}$ . In this figure, panels a)-c) correspond to  $\sin 2\beta = 0.4$ ,  $0.6$ ,  $0.8$  respectively. Panel d) corresponds to the averaged experimental value  $0.80 \pm 0.11$ . Because of the

absolute constraint (2.17),  $R_{sd} \propto 1/(1+f_d)$  and qualitatively figs. 8a and 8b are obtained from figs. 7a and 7b, respectively by subjecting the  $x$ -axis to the transformation  $x \rightarrow 1/x$ . Quantitatively however, the bounds on GMFV models provided by fig. 8 are tighter as they are independent of the poorly known parameter  $F_{B_d} \sqrt{\hat{B}_{B_d}}$ .

### 3 General formulae for $F_{tt}^d$ , $F_{tt}^s$ and $F_{tt}^\varepsilon$ in GMFV Models

Using general formulae (7.27)–(7.32) in [32] it is easy to express the functions  $F_{tt}^d$ ,  $F_{tt}^s$  and  $F_{tt}^\varepsilon$  in terms of the Wilson coefficients at the scale at which the effective Hamiltonian is generated, the relevant QCD renormalization group factors  $\eta$  and the non-perturbative  $B_i$  factors. Suppressing the superscripts  $d$ ,  $s$  and  $\varepsilon$  for a moment we find

$$\begin{aligned} F_{tt} = & \left[ S_0(x_t) + \frac{1}{4r} C_{\text{new}}^{\text{VLL}}(\mu_t) \right] \\ & + \frac{1}{4r} C_1^{\text{VRR}}(\mu_t) + \bar{P}_1^{\text{LR}} C_1^{\text{LR}}(\mu_t) + \bar{P}_2^{\text{LR}} C_2^{\text{LR}}(\mu_t) \\ & + \bar{P}_1^{\text{SLL}} [C_1^{\text{SLL}}(\mu_t) + C_1^{\text{SRR}}(\mu_t)] + \bar{P}_2^{\text{SLL}} [C_2^{\text{SLL}}(\mu_t) + C_2^{\text{SRR}}(\mu_t)] \end{aligned} \quad (3.1)$$

where  $r = 0.985$  [27] describes the QCD corrections to  $S_0(x_t)$  in the SM. This factor is present because we have factored out  $\eta_B$  in (2.5) and  $\eta_2$  in the analogous formula for  $\varepsilon$ . The first line of eq. (3.1) contributes to  $f_{\text{uni}}$  in eq. (2.4) and is therefore present also in the MFV models. The remaining lines are characteristic for the GMFV models and contribute to the  $\tilde{f}_i$  in eq. (2.4). Thus, different values of the functions  $F_{tt}^d$ ,  $F_{tt}^s$  and  $F_{tt}^\varepsilon$  originate from generally different values of the Wilson coefficients  $C_i^a(\mu_t)$  and factors  $\bar{P}_i^a$  pertinent to  $\Delta M_d$ ,  $\Delta M_s$  and  $\varepsilon$ :

$$\bar{P}_i^a = \begin{cases} P_i^a / (4\eta_B \hat{B}_{B_{d,s}}) & (\Delta M_{d,s}) \\ P_i^a / (4\eta_2 \hat{B}_K) & (\varepsilon) \end{cases}, \quad (3.2)$$

where  $\hat{B}_{B_{d,s}}$  and  $\hat{B}_K$  are the relevant non-perturbative parameters related to the matrix elements of  $Q_1^{\text{VLL}}$ .

In the case of  $F_{tt}^{d,s}$  the coefficients  $P_i^a$  are given by

$$P_1^{\text{LR}} = -\frac{1}{2} [\eta_{11}(\mu_b)]_{\text{LR}} [B_1^{\text{LR}}(\mu_b)]_{\text{eff}} + \frac{3}{4} [\eta_{21}(\mu_b)]_{\text{LR}} [B_2^{\text{LR}}(\mu_b)]_{\text{eff}}, \quad (3.3)$$

$$P_2^{\text{LR}} = -\frac{1}{2} [\eta_{12}(\mu_b)]_{\text{LR}} [B_1^{\text{LR}}(\mu_b)]_{\text{eff}} + \frac{3}{4} [\eta_{22}(\mu_b)]_{\text{LR}} [B_2^{\text{LR}}(\mu_b)]_{\text{eff}}, \quad (3.4)$$

$$P_1^{\text{SLL}} = -\frac{5}{8} [\eta_{11}(\mu_b)]_{\text{SLL}} [B_1^{\text{SLL}}(\mu_b)]_{\text{eff}} - \frac{3}{2} [\eta_{21}(\mu_b)]_{\text{SLL}} [B_2^{\text{SLL}}(\mu_b)]_{\text{eff}}, \quad (3.5)$$

$$P_2^{\text{SLL}} = -\frac{5}{8} [\eta_{12}(\mu_b)]_{\text{SLL}} [B_1^{\text{SLL}}(\mu_b)]_{\text{eff}} - \frac{3}{2} [\eta_{22}(\mu_b)]_{\text{SLL}} [B_2^{\text{SLL}}(\mu_b)]_{\text{eff}}. \quad (3.6)$$

with the effective parameters  $[B_i^a(\mu_b)]_{\text{eff}}$  defined by

$$\begin{aligned} [B_i^a(\mu_b)]_{\text{eff}} &\equiv \left( \frac{M_{B_q}}{m_b(\mu_b) + m_q(\mu_b)} \right)^2 B_i^a(\mu_b) \\ &= 1.44 \left[ \frac{4.4 \text{ GeV}}{m_b(\mu_b) + m_q(\mu_b)} \right]^2 \left[ \frac{M_{B_q}}{5.28 \text{ GeV}} \right]^2 B_i^a(\mu_b), \end{aligned} \quad (3.7)$$

where  $B_i^a(\mu_b)$  are related to the hadronic matrix elements  $\langle \bar{B}_q^0 | Q_i | B_q^0 \rangle$ . The QCD factors  $[\eta_{ij}(\mu_b)]_a$  are given in [32].

In the case of  $F_{tt}^\varepsilon$  the QCD factors  $[\eta_{ij}(\mu_b)]_a$  are replaced with  $[\eta_{ij}(\mu_L)]_a$  where  $\mu_L = 2 \text{ GeV}$  and the corresponding effective parameters  $[B_i^a(\mu_L)]_{\text{eff}}$  are defined by

$$[B_i^a(\mu_L)]_{\text{eff}} \equiv \left( \frac{m_K}{m_s(\mu_L) + m_d(\mu_L)} \right)^2 B_i^a(\mu_L) = 18.75 \left[ \frac{115 \text{ MeV}}{m_s(\mu_L) + m_d(\mu_L)} \right]^2 B_i^a(\mu_L). \quad (3.8)$$

The NLO QCD factors  $\eta_{ij}(\mu_b)$  and  $\eta_{ij}(2 \text{ GeV})$ , relevant for  $\Delta M_{d,s}$  and  $\varepsilon$  respectively, have been evaluated in [32]. For completeness we give in table 2 their numerical values for different scales (denoted here by  $\mu_{\text{NP}}$ ) at which the new operators are generated.

The parameters  $B_i$  for the  $\bar{K}^0$ - $K^0$  mixing are known from lattice calculations [31, 41]. For the values corresponding to  $\mu_t$  in the table 2 and in the NDR scheme one finds [32]:

$$\left. \begin{aligned} P_1^{\text{LR}} &= -36.1, & P_2^{\text{LR}} &= 59.3, \\ P_1^{\text{SLL}} &= -18.1, & P_2^{\text{SLL}} &= -32.2, \end{aligned} \right\} \quad \text{for} \quad \mu = 2 \text{ GeV}. \quad (3.9)$$

The large values of these coefficients originate in the strong enhancement of the QCD factors  $\eta_{ij}$  for the LR and SLL (SRR) operators and in the chiral enhancement of their matrix elements seen in eq. (3.8). Consequently even small new physics contributions to  $C_i^{\text{LR}}(\mu_t)$  and  $C_i^{\text{SLL}}(\mu_t)$  can play an important role in the phenomenology [31, 42].

In the case of the  $\bar{B}^0$ - $B^0$  mixing the chiral enhancement of the hadronic matrix elements of the LR and SLL operators is absent. Moreover, the QCD factors  $\eta_{ij}$  are smaller than in the case of the  $\bar{K}^0$ - $K^0$  mixing. Consequently the coefficients  $P_i^{\text{LR}}$  and  $P_i^{\text{SLL}}$  are smaller in this case but can be still important. As lattice results are not yet available for the hadronic matrix elements of the LR and SLL operators in the  $B$  system [43] we will set in this case  $B_i^a(\mu_b) = 1$ . Taking  $M_B = 5.28 \text{ GeV}$ ,  $\mu_b = 4.2 \text{ GeV}$ ,  $m_b(\mu_b) + m_q(\mu_b) = 4.2 \text{ GeV}$  and  $\alpha_s(M_Z) = 0.118$  one finds

$$\left. \begin{aligned} P_1^{\text{LR}} &= -1.65, & P_2^{\text{LR}} &= 2.51, \\ P_1^{\text{SLL}} &= -1.49, & P_2^{\text{SLL}} &= -3.01, \end{aligned} \right\} \quad \text{for} \quad \mu_b = 4.2 \text{ GeV}. \quad (3.10)$$

$\mu_{\text{NP}}$	$\mu_b = 4.2 \text{ GeV}$			$\mu_L = 2 \text{ GeV}$		
	$\mu_t$	500 GeV	1 TeV	$\mu_t$	500 GeV	1 TeV
$[\eta]_{\text{VLL}}$	0.838	0.809	0.793	0.787	0.759	0.744
$[\eta_{11}]_{\text{LR}}$	0.919	0.907	0.902	0.906	0.900	0.898
$[\eta_{12}]_{\text{LR}}$	-0.043	-0.054	-0.060	-0.089	-0.107	-0.118
$[\eta_{21}]_{\text{LR}}$	-0.919	-1.190	-1.360	-1.548	-1.923	-2.159
$[\eta_{22}]_{\text{LR}}$	2.303	2.701	2.951	3.227	3.785	4.136
$[\eta_{11}]_{\text{SLL}}$	1.676	1.846	1.949	2.063	2.272	2.398
$[\eta_{12}]_{\text{SLL}}$	2.049	2.470	2.715	2.970	3.441	3.717
$[\eta_{21}]_{\text{SLL}}$	-0.007	-0.008	-0.009	-0.009	-0.011	-0.012
$[\eta_{22}]_{\text{SLL}}$	0.540	0.480	0.449	0.414	0.366	0.341

Table 2: Numerical values for the  $\eta$ -factors for the  $\bar{B}^0$ - $B^0$  and  $\bar{K}^0$ - $K^0$  mixing for  $\alpha_s^{(5)}(M_Z) = 0.118$  and different values of the scale  $\mu_{\text{NP}}$  at which the New Physics is integrated out.

Since we took  $\mu_b = 4.2 \text{ GeV}$  instead of  $4.4 \text{ GeV}$ , these numbers differ slightly from those given in ref. [32]. Finally in order to calculate  $\hat{P}_i^a$  in (3.2) we will use  $\eta_B = 0.55$ ,  $\eta_2 = 0.57$  and [43]

$$\hat{B}_K = 0.85 \pm 0.15, \quad \hat{B}_{B_{d,s}} = 1.30 \pm 0.18. \quad (3.11)$$

## 4 $F_{tt}^d$ , $F_{tt}^s$ and $F_{tt}^\varepsilon$ in realistic GMVF Models

### 4.1 2HDM(II) with large $\tan \bar{\beta}$

To see what values of  $F_{tt}^d$ ,  $F_{tt}^s$  and  $F_{tt}^\varepsilon$  can be realized in realistic GMVF models we consider here two extensions of the SM. The first is the 2HDM(II) which introduces three neutral physical scalars ( $h^0$ ,  $H^0$  and  $A^0$ ) and a charged physical scalars  $H^\pm$ . At one loop only the charged scalars are relevant for the box diagrams contributing to  $\bar{K}^0$ - $K^0$  and  $\bar{B}^0$ - $B^0$  mixing amplitudes. Using the compact notation of ref. [44] the tree level couplings of  $H_k^+ \equiv (H^+, G^+)$  (where  $G^\pm$  is the would-be Goldstone boson) read

$$L_{\text{int}} = H_k^+ \bar{u}_A V_{AI} (a_L^{AIk} P_L + a_R^{AIk} P_R) d_I + \text{Hc.} \quad (4.1)$$

where

$$a_L^{AIk} = \frac{e}{\sqrt{2}s_W} \frac{m_{u_A}}{M_W} \times \begin{cases} \cot \bar{\beta} & \text{for } k = 1 \\ 1 & \text{for } k = 2 \end{cases} \quad (4.2)$$

$$a_R^{AIk} = \frac{e}{\sqrt{2}s_W} \frac{m_{d_I}}{M_W} \times \begin{cases} \tan \bar{\beta} & \text{for } k = 1 \\ -1 & \text{for } k = 2 \end{cases} \quad (4.3)$$

(Recall that in our notation  $d_3 \equiv b$ ,  $d_2 \equiv s$ ,  $d_1 \equiv d$  and, analogously,  $u_3 \equiv t$ ,  $u_2 \equiv c$ ,  $u_1 \equiv u$ .) Contribution of  $H_k^\pm$  to the Wilson coefficients  $C_i$  of the operators responsible for the transition  $d_I \bar{d}_J \rightarrow \bar{d}_I d_J$  in eq. (2.1) can be easily expressed in terms of the coefficients  $a_L^{AIk}$  and  $a_R^{AIk}$ . Diagrams with one  $W^\pm$  and one  $H^\pm$  give<sup>§</sup>:

$$\begin{aligned} G_F^2 M_W^2 \delta^{(+)} C_1^{\text{VLL}}(\mu_{\text{NP}}) &= -\frac{e^2}{2s_W^2} a_L^{tJ1} a_L^{tI1} m_t^2 D_0(M_W, M_{H^+}, m_t, m_t) \\ G_F^2 M_W^2 \delta^{(+)} C_2^{\text{LR}}(\mu_{\text{NP}}) &= -\frac{e^2}{2s_W^2} \sum_{k=1}^2 a_R^{tJk} a_R^{tIk} \left[ D_2(M_W, M_{H_k^+}, m_t, m_t) \right. \\ &\quad \left. - 2D_2(M_W, M_{H_k^+}, m_t, 0) + D_2(M_W, M_{H_k^+}, 0, 0) \right] \end{aligned} \quad (4.4)$$

where the four-point functions  $D_0$  and  $D_2$  are defined in the Appendix. Diagrams with two  $H_k^\pm$  give<sup>¶</sup>:

$$\begin{aligned} G_F^2 M_W^2 \delta^{(+)} C_1^{\text{VLL}}(\mu_{\text{NP}}) &= \frac{1}{8} \sum_{k,l} a_L^{tJl} a_L^{tIk} a_L^{tJk} a_L^{tIl} D_2(M_{H_l^+}, M_{H_k^+}, m_t, m_t) \\ G_F^2 M_W^2 \delta^{(+)} C_1^{\text{VRR}}(\mu_{\text{NP}}) &= \frac{1}{8} \sum_{k,l}^2 a_R^{tJl} a_R^{tIk} a_R^{tJk} a_R^{tIl} \left[ D_2(M_{H_l^+}, M_{H_k^+}, m_t, m_t) \right. \\ &\quad \left. - 2D_2(M_{H_l^+}, M_{H_k^+}, m_t, 0) + D_2(M_{H_l^+}, M_{H_k^+}, 0, 0) \right] \\ G_F^2 M_W^2 \delta^{(+)} C_1^{\text{LR}}(\mu_{\text{NP}}) &= \frac{1}{4} \sum_{k,l}^2 a_L^{tJl} a_L^{tIk} a_R^{tJk} a_R^{tIl} D_2(M_{H_l^+}, M_{H_k^+}, m_t, m_t) \\ G_F^2 M_W^2 \delta^{(+)} C_1^{\text{SLL}}(\mu_{\text{NP}}) &= \frac{1}{2} \sum_{k,l}^2 a_R^{tJl} a_L^{tIk} a_R^{tJk} a_L^{tIl} m_t^2 D_0(M_{H_l^+}, M_{H_k^+}, m_t, m_t) \\ G_F^2 M_W^2 \delta^{(+)} C_1^{\text{SRR}}(\mu_{\text{NP}}) &= \frac{1}{2} \sum_{k,l}^2 a_L^{tJl} a_R^{tIk} a_L^{tJk} a_R^{tIl} m_t^2 D_0(M_{H_l^+}, M_{H_k^+}, m_t, m_t) \\ G_F^2 M_W^2 \delta^{(+)} C_2^{\text{LR}}(\mu_{\text{NP}}) &= \sum_{k,l}^2 a_R^{tJl} a_L^{tIk} a_L^{tJk} a_R^{tIl} m_t^2 D_0(M_{H_l^+}, M_{H_k^+}, m_t, m_t) \end{aligned} \quad (4.5)$$

<sup>§</sup>The contribution of  $G^\pm$  to  $C_1^{\text{VLL}}$  is already taken into account in the function  $S_0(x_t)$ . Masses of the  $u$  and  $c$  quarks are neglected.

<sup>¶</sup>In the sum over  $k$  and  $l$  in the expression for  $\delta^{(+)} C_1^{\text{VLL}}$  the contribution of  $G^\pm G^\mp$  is excluded. It is taken into account in the function  $S_0(x_t)$ .

At one loop there are no contributions to the Wilson coefficients of the tensor operators  $Q_2^{\text{SLL}}$  and  $Q_2^{\text{SRR}}$ . In the computations we take  $\mu_{\text{NP}} = M_{H^+}$  and apply the formulae given in Appendix C of ref. [32]. As our calculation of the Wilson coefficients at  $\mu_{\text{NP}}$  does not include  $\mathcal{O}(\alpha_s)$  corrections and the relevant matrix elements of LR and SLL operators in the  $B$ -system have been evaluated using the vacuum insertion method, there are inevitably unphysical scale and renormalization scheme dependences present in our final results. We expect that these dependences are small at scales  $\mathcal{O}(\mu_{\text{NP}})$  as the strong coupling  $\alpha_s(\mu_{\text{NP}})$  is small. They could turn out to be more important at  $\mu = \mu_b$  where  $\alpha_s$  is bigger. Consequently the evaluation of the hadronic matrix elements of the LR and SLL operators relevant for  $\bar{B}^0$ - $B^0$  mixing in the NDR scheme is very desirable. This would not only remove the unphysical dependences in question but would also give the actual values of the relevant matrix elements in QCD. Still we believe that our calculation captures the correct size of the dominant new physics effects.

For large  $\tan \bar{\beta}$  and  $M_{H^+} \approx m_t$  the leading terms of the above contributions to the Wilson coefficients  $C_i$  are of the order  $(e^4/(32s_W^4 M_W^2) = G_F^2 M_W^2)$ :

$$\delta^{(+)} C_1^{\text{VLL}} \sim \frac{4}{3} \cot^2 \bar{\beta}, \quad \delta^{(+)} C_2^{\text{LR}} \sim -\frac{8}{3} \frac{m_{d_I} m_{d_J}}{m_t^2} \tan^2 \bar{\beta} \quad (4.6)$$

for diagrams with  $W^\pm H^\mp$ , and

$$\begin{aligned} \delta^{(+)} C_1^{\text{VLL}} &\sim \frac{1}{3} \frac{m_t^2}{M_W^2} \cot^2 \bar{\beta}, & \delta^{(+)} C_1^{\text{VRR}} &\sim \frac{1}{3} \frac{m_{d_I}^2 m_{d_J}^2}{M_W^2 m_t^2} \tan^4 \bar{\beta}, & \delta^{(+)} C_1^{\text{LR}} &\sim 0 \\ \delta^{(+)} C_1^{\text{SLL}} &\sim 0, & \delta^{(+)} C_1^{\text{SRR}} &\sim 0, & \delta^{(+)} C_2^{\text{LR}} &\sim -\frac{4}{3} \frac{m_{d_I} m_{d_J}}{M_W^2} \tan^2 \bar{\beta} \end{aligned} \quad (4.7)$$

for diagrams with  $H^\pm H^\mp$ . It is clear that for large  $\tan \bar{\beta}$  the biggest contribution appears in  $\delta^{(+)} C_2^{\text{LR}}$ . It is of the opposite sign than the contribution of the  $tW^\pm$  box diagram and can be significant only for the  $\bar{B}_s^0$ - $B_s^0$  transition amplitude for which it is of the order

$$\delta^{(+)} C_2^{\text{LR}} \approx -\frac{2m_s(\mu_t) m_b(\mu_t)}{M_W^2} \tan^2 \bar{\beta} \approx -0.14 \times \left( \frac{\tan \bar{\beta}}{50} \right)^2 \quad (4.8)$$

where we have used  $m_b(\mu_t) \approx 3$  GeV and  $m_s(\mu_t) \approx 61$  MeV. Compared to the estimate of eq. (4.8), similar contributions to  $\delta^{(+)} C_2^{\text{LR}}$  for  $\bar{B}_d^0$ - $B_d^0$  and  $\bar{K}^0$ - $K^0$  transitions are suppressed by factors  $m_d/m_s$  and  $m_d/m_b$ , respectively. As discussed in Sec. 3 all these contributions are further enhanced compared to the standard ones by the QCD renormalization effects and, in the case of the  $\bar{K}^0$ - $K^0$  transition, also by the chiral enhancement of the corresponding matrix element. As a result, in the case of  $\bar{B}_s^0$ - $B_s^0$  mixing the contribution of the  $Q_2^{\text{LR}}$  operator can compete with the contribution of the standard  $Q_1^{\text{VLL}}$  one for light charged Higgs boson and large values of  $\tan \bar{\beta}$ . To demonstrate it we plot in

fig. 9 the value of  $1 + f_s$  in 2HDM(II) for different values of its parameters. Fig. 9a shows that a significant decrease of  $1 + f_s$  below unity is possible only for  $M_{H^+} \sim 100 - 200$  GeV and  $\tan \bar{\beta}$  close to its upper limit following from the requirement of perturbativity of the bottom quark Yukawa coupling. The corresponding effects in  $1 + f_d$  and  $1 + f_\varepsilon$  are negligible. The increase of  $1 + f_s$  above unity seen in fig. 9a for  $\tan \bar{\beta} < 10$  reflects a well known universal contribution of the box diagrams to the Wilson coefficient of the  $Q_1^{\text{VLL}}$  operator which gives  $1 + f_s \approx 1 + f_d \approx 1 + f_\varepsilon > 1$ .

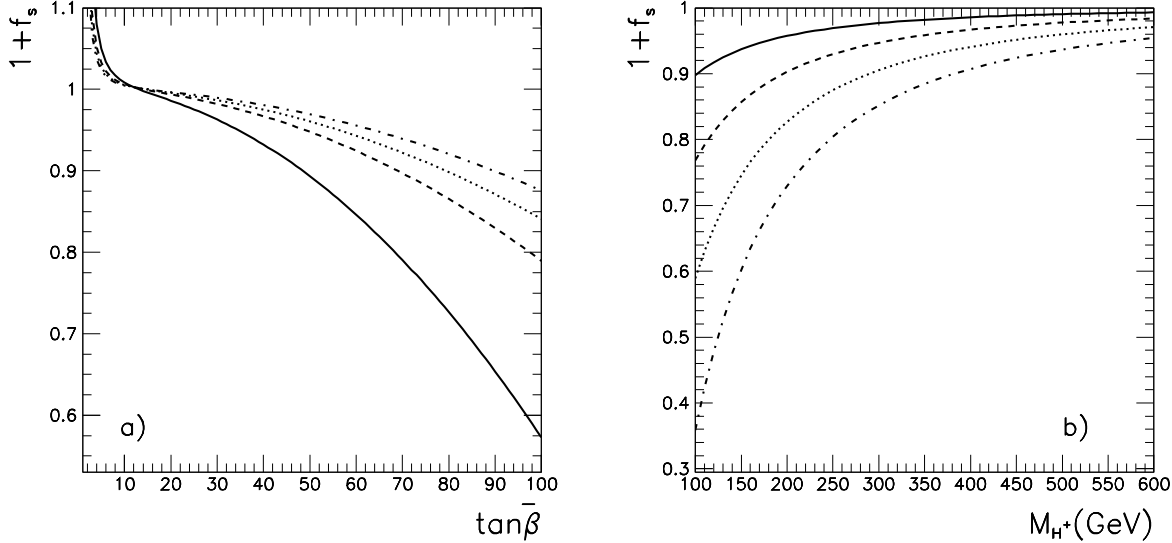


Figure 9:  $1 + f_s$  in the 2HDM(II): a) as a function of  $\tan \bar{\beta}$  for  $M_{H^+} =$  (from below) 150, 250, 300 and 350 GeV and b) as a function of  $M_{H^+}$  for  $\tan \bar{\beta} =$  (from above) 40, 60, 80 and 100.

Unfortunately, recent refinements in the computation of the  $b \rightarrow s\gamma$  rate [45] together with the new CLEO experimental result for this process [46]  $BR(B \rightarrow X_s\gamma) = (3.03 \pm 0.40 \pm 0.26) \times 10^{-4}$  set the bound  $M_{H^+} \gtrsim 380$  GeV [47, 45]. This means that in the 2HDM(II) for the still allowed range of charged Higgs boson masses the decrease of  $1 + f_s$  can be very small. Consequently, the SM analysis of the unitarity triangle based on  $\varepsilon$ ,  $\Delta M_d$  and  $\Delta M_s$  is practically unchanged in the 2HDM(II) for large  $\tan \bar{\beta} \lesssim 50$ .

However, the bound on  $M_{H^+}$  from the  $b \rightarrow s\gamma$  rate does not apply in the MSSM which we consider in the next subsection.

## 4.2 MSSM with large $\tan\bar{\beta}$

As a second realistic GMFV model we consider the MSSM. At the one loop level the contributions to the Wilson coefficients of the  $|\Delta F| = 2$  operators (2.2) in the MSSM are given<sup>||</sup> by chargino-top squark box diagrams and by box diagrams with the charged Higgs boson. Since the Higgs sector of the MSSM is (at the tree level) a special case of the general 2HDM(II) considered in subsection 4.1, the latter contribution is described by the formulae (4.4), (4.5). It is well known [24, 25, 48] that for  $\tan\bar{\beta}$  not too big, the MSSM is of the MFV type and both, the chargino-stop and the Higgs sectors give *positive* contributions to  $1 + f_s \approx 1 + f_d \approx 1 + f_\varepsilon$  which are the bigger the lighter are particles in the loops and the smaller is the value of  $\tan\bar{\beta}$ . In this section we want to consider the MSSM with large values of  $\tan\bar{\beta}$  which are favoured both by the LEP limit on the mass of the lighter neutral Higgs boson and by the recent measurement of the anomalous magnetic moment of the muon [49]. As the treatment of the full MSSM contribution is complicated, we will for simplicity consider here only the limit of heavy sparticles and will concentrate only on the most spectacular effects. Complete analysis of the MSSM will be presented elsewhere [26].

In the limit of heavy sparticles (which is practically realized already for  $M_{\text{sparticles}} \gtrsim 500$  GeV) the one loop diagrams involving charginos and stops are negligible. It is however known that for large  $\tan\bar{\beta}$  even if sparticles are heavy they can still compensate the  $H^\pm$  contribution to the  $b \rightarrow s\gamma$  amplitude allowing for the existence of a light,  $\sim \mathcal{O}(150 \text{ GeV})$ , charged Higgs boson [50, 51]. From fig. 9 it follows therefore that, even for<sup>\*\*</sup>  $\tan\bar{\beta} \lesssim 50$  and already at the one loop level the contribution of the MSSM Higgs sector to the  $C_2^{\text{LR}}$  Wilson coefficient can be non-negligible.

At the two loop level one has to take into account not only the  $\mathcal{O}(\alpha_s)$  corrections to the Wilson coefficients (which in the MSSM arise from exchanges of gluons as well as gluinos) but also the dominant two loop electroweak corrections (proportional to large top and, in the case of large  $\tan\bar{\beta}$ , bottom Yukawa couplings). The gluonic  $\mathcal{O}(\alpha_s)$  corrections to the charged Higgs box diagrams are expected to be of the same order of magnitude as the gluonic correction to the SM  $t - W^\pm$  box diagrams, i.e. moderate [28]. Also most of the two loop diagrams involving sparticles will give contributions suppressed by the inverse of the large sparticle masses. The one loop effects of the MSSM Higgs sector are however enhanced by an important class of two loop corrections involving sparticles. In the limit of heavy sparticles these corrections can be most easily identified in the effective

---

<sup>||</sup>In accordance with the general framework of this paper we assume here that the CKM matrix is the only source of flavour and CP violation.

<sup>\*\*</sup>In the MSSM one usually constrains  $\tan\bar{\beta}$  to be less than  $50 - 55$  by requiring perturbativity of the Yukawa couplings up to the GUT scale  $\sim 10^{16}$  GeV.

Lagrangian approach [52]. While direct contribution of heavy sparticles to the Wilson coefficients can be neglected, it is well known that for large  $\tan \bar{\beta}$  such sparticles do not decouple entirely [53]. Integrating them out modifies the original couplings of the two Higgs doublets to the known fermions leading to the following quark Yukawa interactions:

$$\begin{aligned} \mathcal{L}_{\text{Yuk}} = & -\epsilon_{ij} H_i^{(d)} d_I^c Y_d^{IA} q_{Aj} - H_i^{(u)*} d_I^c (\Delta_u Y_d)^{IA} q_{Ai} \\ & - \epsilon_{ij} H_i^{(u)} u_A^c Y_u^{AI} q_{Ij} - H_i^{(d)*} u_A^c (\Delta_d Y_u)^{AI} q_{Ii} + \text{H.c.} \end{aligned} \quad (4.9)$$

where  $H_i^{(d)}$  and  $H_i^{(u)}$  are the two Higgs doublets giving at the tree level masses to the down- and up-type quarks, respectively and  $q_i$ ,  $d^c$  and  $u^c$  are the fields of the left handed fermions (for simplicity we use here the Weyl spinors). Dominant corrections  $(\Delta_u Y_d)^{IA}$  and  $(\Delta_d Y_u)^{AI}$  are finite and calculable in terms of the sparticle parameters. In the effective Lagrangian approach they can be obtained from diagrams shown in fig. 10 in which  $Q$ ,  $U^c$  and  $D^c$  are the scalar superpartners of the SM fermions  $q_i$ ,  $d^c$  and  $u^c$ ,  $\tilde{g}$  is the gluino and  $\tilde{H}_i^{(d)}$  and  $\tilde{H}_i^{(u)}$  are the fermionic superpartners of the two Higgs doublets.

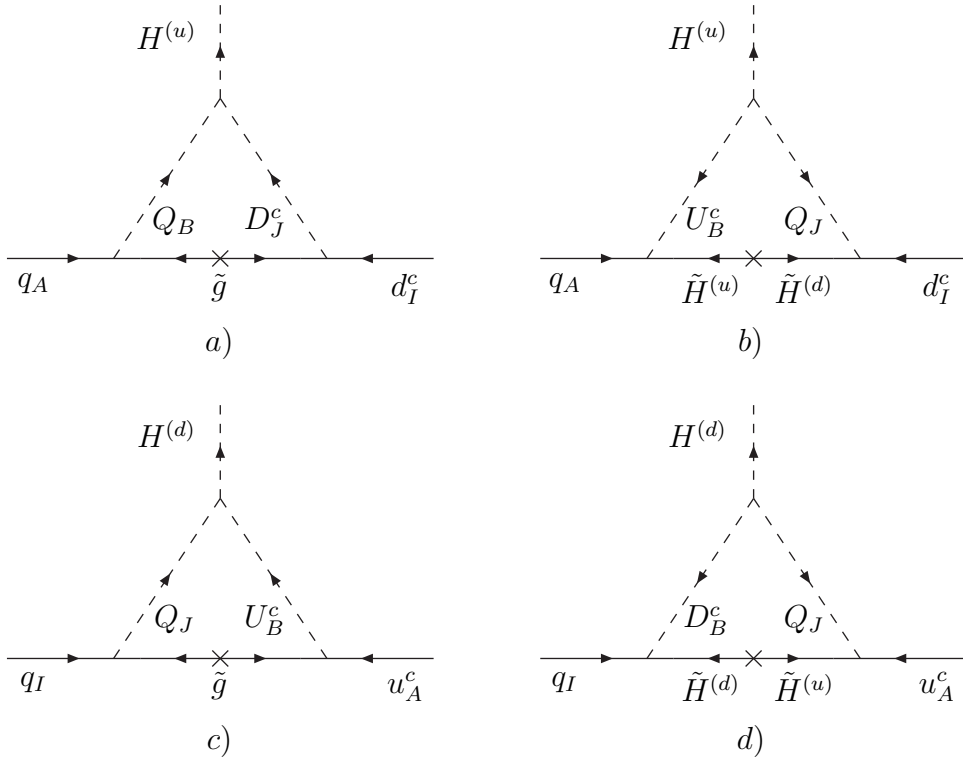


Figure 10: Diagrams giving rise to dominant,  $\tan \bar{\beta}$  enhanced, corrections  $\Delta_u Y_d$  (diagrams a and b) and  $\Delta_d Y_u$  (diagrams c and d).

The effects of the corrections  $\Delta Y$  are threefold. Firstly, they modify the 2HDM(II)

relations between the masses  $m_{d_I}(\mu_t)$  and the eigenvalues of the Yukawa matrices  $Y_d^{IA}$ :

$$Y_d^I = \frac{e}{\sqrt{2}s_W} \frac{m_{d_I}}{M_W} \sqrt{1 + \tan^2 \bar{\beta}} \rightarrow \frac{e}{\sqrt{2}s_W} \frac{m_{d_I}}{M_W} \frac{\sqrt{1 + \tan^2 \bar{\beta}}}{1 + \epsilon_d(I) \tan \bar{\beta}} \quad (4.10)$$

where  $\epsilon_d(I)$  can be found in ref. [50]. Secondly, they induce additional,  $\propto \tan \bar{\beta}$ , terms in the couplings (4.2), (4.3) [22, 50]. Both these corrections should be taken into account in vertices of the charged Higgs boson box diagrams and constitute, therefore, the two loop corrections to the Wilson coefficients of the  $|\Delta F| = 2$  operators. It turns out, however, that the most important (for non-negligible mixing of the top squarks) effect of the corrections  $\Delta Y$  is the generation of the flavour non-diagonal,  $\tan \bar{\beta}$  enhanced couplings of the neutral Higgs bosons to down-type quarks [54, 55]. In the effective Lagrangian approach these couplings originate from the diagram 10b. Details of their calculation have been presented in ref. [56]. They can be also computed diagrammatically as in [56, 57] what allows to take fully into account the complicated composition of charginos. Additional contributions to the Wilson coefficients  $C_1^{\text{SLL}}$ ,  $C_1^{\text{SRR}}$  and  $C_2^{\text{LR}}$  are then generated by the double penguin diagrams shown in fig. 11 in which the neutral Higgs bosons are exchanged at the tree level between two effective flavour changing vertices generated at one loop.

The single neutral Higgs penguin diagram for the  $(d_I)_{\text{L(R)}} \rightarrow (d_J)_{\text{R(L)}}$  transition (where L and R refer to the quark chiralities) grows as  $\tan^2 \bar{\beta}$  and is proportional to  $m_{d_J}$  ( $m_{d_I}$ ) [56]. Consequently the double penguin diagrams in fig. 11 grow like  $\tan^4 \bar{\beta}$  times  $m_{d_J}^2$ ,  $m_{d_I}^2$  and  $m_{d_J} m_{d_I}$ , respectively. This mismatch of powers in  $\tan \bar{\beta}$  and powers of light quark masses in Higgs penguin diagrams should be contrasted with box diagrams, where each  $\tan \bar{\beta}$  is accompanied by a light quark mass as seen in (4.6)-(4.8). In this manner the two-loop electroweak double Higgs penguins can potentially compete with the one loop electroweak box diagrams. In the standard diagrammatic approach to the calculation of the flavour changing  $d_J d_I H^0(h^0, A^0)$  vertex the mismatch of powers in question can be understood simplest as follows. The diagrams for the genuine 1-PI vertex corrections (with physical squarks and charginos in the loops) contribute only terms proportional to one power of  $\tan \bar{\beta}$ . They are however accompanied by two tree level flavour conserving  $d_J d_J$ -Higgs and  $d_I d_I$ -Higgs vertices with flavour violating self-energies (involving squarks and charginos) on the external quarks lines. As the external momenta can be neglected, the internal fermion propagators of  $d_J$  and  $d_I$  cancel respectively the  $m_{d_J}$  and  $m_{d_I}$  factors present in the quark-quark-Higgs vertices.

For the transitions  $d_I \bar{d}_J \rightarrow d_J \bar{d}_I$  the dominant terms obtained from the double penguin contributions are

$$\delta^{(0)} C_1^{\text{SLL}} = -\frac{\alpha_{EM}}{4\pi s_W^2} \frac{m_t^4}{M_W^4} m_{d_J}^2 X_{tC}^2 \tan^4 \bar{\beta} \mathcal{F}_- \quad$$

$$\begin{aligned}\delta^{(0)}C_1^{\text{SRR}} &= -\frac{\alpha_{EM}}{4\pi s_W^2} \frac{m_t^4}{M_W^4} m_{d_I}^2 X_{tC}^2 \tan^4 \bar{\beta} \mathcal{F}_- \\ \delta^{(0)}C_2^{\text{LR}} &= -\frac{\alpha_{EM}}{2\pi s_W^2} \frac{m_t^4}{M_W^4} m_{d_J} m_{d_I} X_{tC}^2 \tan^4 \bar{\beta} \mathcal{F}_+.\end{aligned}\quad (4.11)$$

$X_{tC}$  is given by

$$X_{tC} = \sum_{j=1}^2 Z_+^{2j} Z_-^{2j} \frac{A_t}{m_{C_j}} H_2(x_1^{t/C_j}, x_2^{t/C_j}), \quad (4.12)$$

where  $x_i^{t/C_j} = M_{\tilde{t}_i}/m_{C_j}^2$ ,  $i = 1, 2$ ,  $j = 1, 2$  are the ratios of the stop and chargino masses squared, the matrices  $Z_+$  and  $Z_-$  are defined in ref. [44] and the function  $H_2(x, y)$  is defined in the Appendix. The factor

$$\mathcal{F}_\mp \equiv \left[ \frac{\cos^2 \bar{\alpha}}{M_H^2} + \frac{\sin^2 \bar{\alpha}}{M_h^2} \mp \frac{\sin^2 \bar{\beta}}{M_A^2} \right] \quad (4.13)$$

depends on the masses of the CP-even neutral Higgs bosons  $h^0$  and  $H^0$ , the mass of the CP-odd Higgs boson  $A^0$  (in the MSSM  $M_{H^+}^2 = M_A^2 + M_W^2$ ) and the mixing angles  $\bar{\alpha}$  and  $\bar{\beta}$ . For  $\tan \bar{\beta} \gg 1$  and  $M_A \gtrsim 130$  GeV,  $\cos^2 \bar{\alpha} \approx 1$ ,  $\sin^2 \bar{\alpha} \approx 0$  and  $M_H \approx M_A$ .

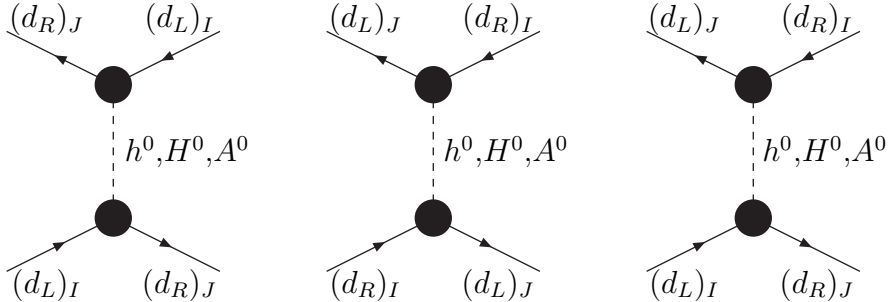


Figure 11: Double penguin diagram contributing to: a)  $C_1^{\text{SLL}}$ , b)  $C_1^{\text{SRR}}$  and c)  $C_2^{\text{LR}}$  Wilson coefficients in the MSSM with large  $\tan \bar{\beta}$ .

As has been observed in [55],  $\delta^{(0)}C_1^{\text{SLL}}$  and  $\delta^{(0)}C_1^{\text{SRR}}$  depend on  $\mathcal{F}_-$  which for  $\tan \bar{\beta} \gg 1$  is close to zero and strongly suppresses these corrections. However the correction  $\delta^{(0)}C_2^{\text{LR}}$  is proportional to  $\mathcal{F}_+$  which is not suppressed in this limit. Approximating for simplicity the dimensionless factor  $X_{tC}$  by unity, it is easy to see that in the case of the  $\bar{B}_s^0$ - $B_s^0$  mixing this correction, although proportional to small strange quark mass ( $m_s(\mu_t) \approx 61$  MeV), can be for  $\tan \bar{\beta} \sim 50$  and  $M_{H^+} \sim 200$  GeV as large as  $\delta^{(0)}C_2^{\text{LR}} \sim 2.5$  i.e. of the same order of magnitude as the SM contribution to  $C_1^{\text{VLL}}$ . Consequently there can be a significant, growing as  $\tan^4 \bar{\beta}$ , contribution to the  $C_2^{\text{LR}}$  Wilson coefficient which is further enhanced (relative to the  $C_1^{\text{VLL}}$  coefficient) by QCD effects (see sec. 3).

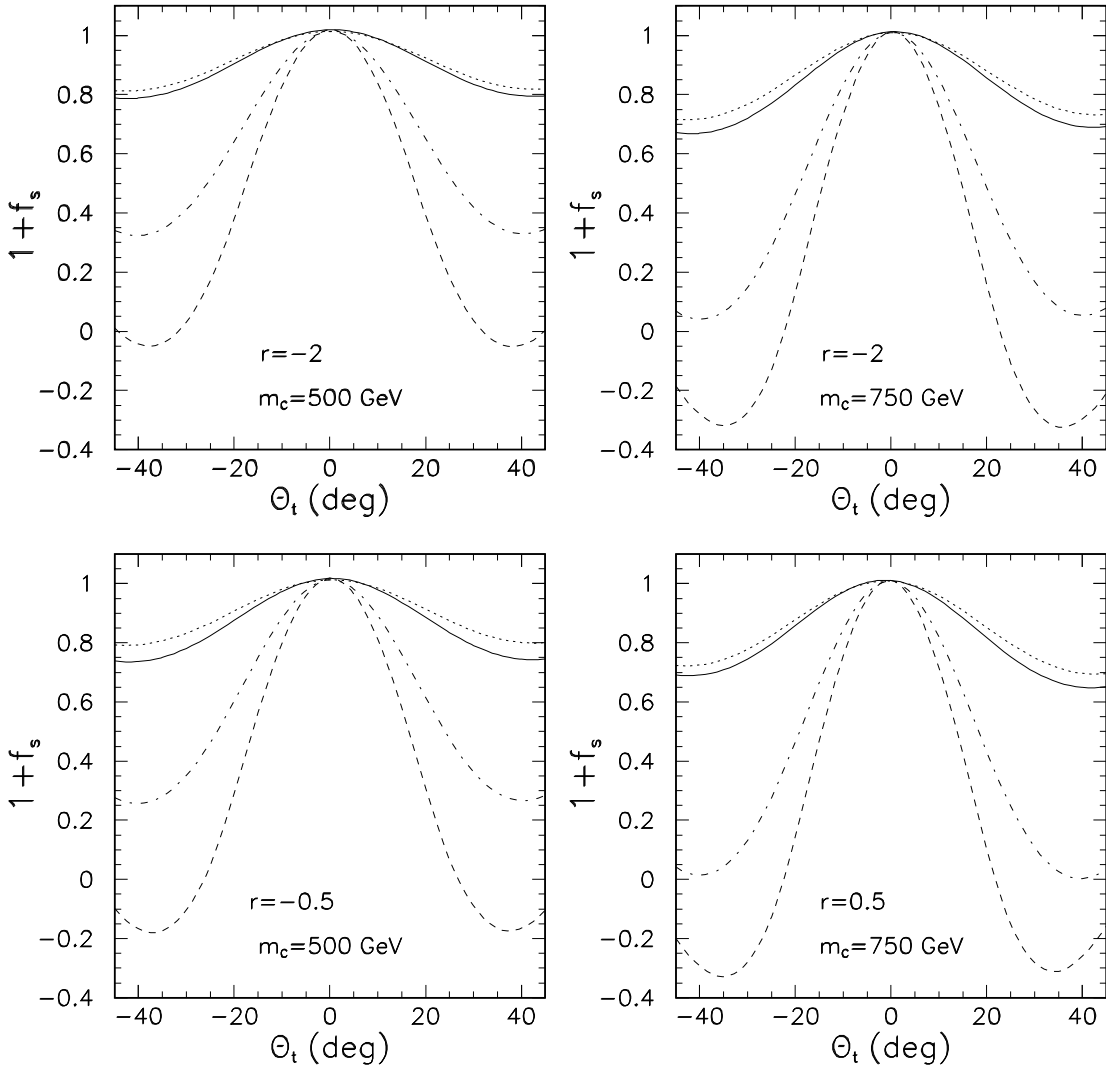


Figure 12:  $1 + f_s$  in the MSSM as a function of the mixing angle of the top squarks for different lighter chargino masses and compositions ( $r \equiv M_2/\mu$ ). Solid, dashed, dotted and dot-dashed lines correspond to stop masses (in GeV) (500,650), (500,850), (700,850) and (700,1000), respectively.

An important feature of the double penguin contribution is its fixed negative sign (because it is proportional  $X_{tC}^2$ ) i.e. the same as the sign of the dominant effects of the charged Higgs box diagrams at large  $\tan \bar{\beta}$ . Therefore the double penguin contribution interferes destructively with the SM contribution and leads to  $1 + f_s < 1$ . Another

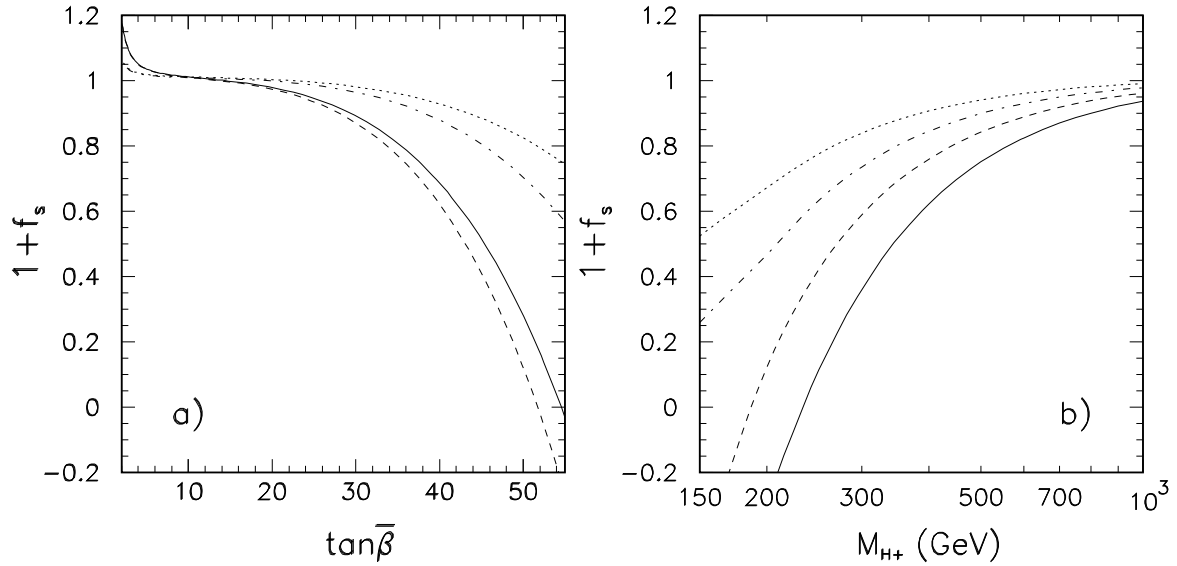


Figure 13:  $1 + f_s$  in the MSSM for lighter chargino mass 750 GeV,  $r \equiv M_2/\mu = -0.5$  and stop masses (in GeV) (500,850), (700,1000), (500,850) and (600,1100) (solid, dashed, dotted and dot-dashed lines, respectively) as a function of a)  $\tan \bar{\beta}$  and b)  $M_{H^+}$ . In panel a) solid and dashed (dotted and dot-dashed) lines correspond to  $M_{H^+} = 200$  (600) GeV, and in panel a) solid and dashed (dotted and dot-dashed) lines correspond to  $\tan \bar{\beta} = 50$  (35).

interesting feature is its strong dependence on the left-right mixing of the top squarks which is clearly visible in fig. 12 where we show  $1 + f_s$  as a function of the stop mixing angle  $\theta_t$  for different chargino masses and compositions and different choices of the stop masses. For the same value of the mixing angle  $\theta_t$ , larger effects are obtained for bigger stop mass splitting because in this case the parameter  $|A_t|$  has to be larger. It should be also stressed that this contribution does not vanish when the mass scale of the sparticles is increased (i.e. when all mass parameters are scaled uniformly). Thus, large effects decreasing  $1 + f_s$  below unity can be present in the MSSM also for the heavy sparticles provided the mass scale of the MSSM Higgs sector remains low and  $\tan \bar{\beta}$  is large. This is illustrated in figs. 13a and b where we show  $1 + f_s$  as a function of  $\tan \bar{\beta}$  (panel a) and  $M_{H^+}$  (panel b). Positive contribution to  $1 + f_s$  seen in fig. 13a for  $\tan \bar{\beta} < 2.5$  and  $M_{H^+} = 200$  GeV is due to the ordinary charged Higgs box diagrams which contribute to the universal part of  $f_s$ ,  $f_d$  and  $f_\epsilon$  through the Wilson coefficient of the standard  $Q_1^{\text{VLL}}$  operator. For lighter  $H^+$  and light charginos  $1 + f_s$  can reach values  $\sim 2$  [25]. As follows

from (2.18) such high values of  $1 + f_s$  could be soon excluded by the measurement of  $\Delta M_s$ .

The implications of these results are as follows. A large portion of the MSSM parameter space considered here leads to  $1 + f_s$  values violating already at present the bound (2.18) and is, hence, excluded. It is particularly interesting that part of this parameter space is not yet excluded by the recent results for the  $b \rightarrow s\gamma$  rate. This is because the theoretical prediction for the latter depends, besides stop and chargino sector parameters (on which the double penguin contribution does depend), also on masses of sfermions from the first two generations, the gluino mass etc. This can have important consequences for other processes involving the  $B^0$  mesons. For instance, orders of magnitude enhancement of the  $B_{s,d}^0 \rightarrow \mu^+ \mu^-$  branching ratio found in the MSSM for very large mixing of stops [55, 56, 57, 58] is ruled out, at least for sparticles so heavy that their direct contribution to the  $\bar{B}_s^0$ - $B_s^0$  mixing cannot significantly reduce the negative double penguin contribution to  $1 + f_s$ . Thus, finding  $BR(B_{s,d}^0 \rightarrow \mu^+ \mu^-)$  close to the present experimental bound and no light stops and charginos would strongly indicate a non-minimal flavour violation in supersymmetry [56].

Furthermore, for the MSSM parameters, for which the bound (2.18) is respected,  $1 + f_d \approx 1 + f_\varepsilon \approx 1$  and in this sector the MSSM in the limit  $M_W \lesssim M_{H^+} \ll M_{\text{sparticle}}$  mimics the SM. In particular, it is still consistent with the present experimental data for  $\varepsilon$ ,  $\Delta M_d$ ,  $\Delta M_s$  and  $a_{\psi K_S}$ . Measuring  $\Delta M_s$  larger than the present lower bound  $\Delta M_s > 15/ps$  will further limit allowed combinations of stop mixings, their mass splittings and chargino parameters. Only very large values of  $\Delta M_s$ , requiring  $1 + f_s \gtrsim 1$ , would rule out the supersymmetric scenario considered here entirely; the SM would be then ruled out too.

Obviously, finding the asymmetry  $a_{\psi K_S}$  below its SM value would also rule out this scenario entirely because for  $1 + f_d \approx 1 + f_\varepsilon \approx 1$  the unitarity of the CKM matrix requires  $\sin 2\beta \gtrsim 0.5$ , i.e. bigger than the bound (1.6) valid in MVF models which admit  $1 + f_d \approx 1 + f_\varepsilon \neq 1$ . If  $a_{\psi K_S}$  is found around 0.6 then the combination of constraints from  $R_b$ ,  $\varepsilon$  and  $\sin 2\beta$  similar to the ones shown in fig. 8 can put slightly stronger limits on  $1 + f_s \approx R_{sd}$  than the bound (2.18) alone but the usefulness of this limits will depend crucially on the measured value of  $\Delta M_s$ .

Finally, if experimentally  $a_{\psi K_S} \approx 0.7$  and  $\Delta M_s$  combined with improved lattice results for  $\sqrt{\hat{B}_{B_s}} F_{B_s}$  and  $\xi$  allow for  $R_{sd} \approx 1 + f_s \sim 0.65 - 0.8$ , this scenario can lead to angle  $\gamma$  moderately smaller than the one predicted in the SM.

## 5 Conclusions

In this paper we have investigated the role of new dimension six four-fermion  $|\Delta F| = 2$  operators in models with minimal flavour violation. Short distance contributions to the mass differences  $\Delta M_s$ ,  $\Delta M_d$  and to the CP violation parameter  $\varepsilon$  are parameterized by three real functions  $F_{tt}^s$ ,  $F_{tt}^d$  and  $F_{tt}^\varepsilon$ , respectively. General formulae for  $F_{tt}^i$  in terms of the Wilson coefficients evaluated at the scale  $\mu = \mu_{\text{NP}}$ , the relevant QCD renormalization group factors and the non-perturbative  $B_i$ -factors have been presented.

We have proposed a few simple strategies involving the ratio  $\Delta M_s/\Delta M_d$ ,  $\sin 2\beta$  and the angle  $\gamma$  that allow to search for the effects of the new operators. We have also found model independent bounds on the functions  $1 + f_i = F_{tt}^i/S_0(x_t)$  that should be considerably improved once  $\Delta M_s/\Delta M_d$ ,  $\sin 2\beta$  and the angle  $\gamma$  are precisely measured and our knowledge about non-perturbative parameters and the CKM elements  $|V_{ub}|$  and  $|V_{cb}|$  is improved. Our findings can be summarized as follows:

- The present experimental and theoretical uncertainties allow for sizable contributions of new operators to  $\Delta M_{s,d}$  and  $\varepsilon$ .
- As the unitarity of the CKM matrix implies  $|V_{ts}| \approx |V_{cb}|$  independently of new physics contributions, the function  $1 + f_s$  can be determined from the experimental value of  $\Delta M_s$  subject to the uncertainties in  $|V_{cb}|$ ,  $m_t$  and in particular  $\sqrt{\hat{B}_{B_s}} F_{B_s}$ . For instance for  $\Delta M_s = 18/\text{ps}$  we find  $0.63 \leq 1 + f_s \leq 1.55$ . The decrease of the theoretical error in  $\sqrt{\hat{B}_{B_s}} F_{B_s}$  accompanied by a precise measurement of  $\Delta M_s$  should tell us whether  $1 + f_s > 1$  or  $1 + f_s < 1$  thereby excluding certain scenarios and putting important constraints on the parameter space of the surviving models.
- We find that values of  $R_{sd} = (1 + f_s)/(1 + f_d)$  substantially different from unity would allow  $\sin 2\beta$  to be lower than in the MFV models and in particular in the SM. Simultaneously  $R_{d\varepsilon} = (1 + f_d)/(1 + f_\varepsilon) < 1$  would be favoured.
- Whether  $R_{sd} > 1$  or  $R_{sd} < 1$  is favoured by the data can be decided by the measurement of the angle  $\gamma$  with  $\gamma > 90^\circ$  and  $\gamma < 90^\circ$  corresponding for  $\Delta M_s = 15/\text{ps}$  to  $R_{sd} > 1.2$  and  $R_{sd} < 1.2$ , respectively. For a given  $R_{sd}$  and  $\sin 2\beta$ , the predicted angle  $\gamma$  decreases with increasing  $\Delta M_s$ . For  $R_{sd} > 1.5$  and  $\Delta M_s/\Delta M_d \leq 40$  values of the angle  $\gamma$  greater than  $90^\circ$  are possible.
- We have determined the presently allowed ranges in the  $(1 + f_d, 1 + f_\varepsilon)$  and  $(R_{sd}, 1 + f_\varepsilon)$  planes. An analysis of a hypothetical measurements of  $\Delta M_s$  and  $a_{\psi K_s}$  that allow the determination of the unitarity triangle illustrated various possibilities further.

As an example we have analyzed the role of new operators in the MSSM with large  $\tan \bar{\beta} = v_2/v_1$  in the limit of heavy sparticles, investigating in particular the impact of the extended Higgs sector on the unitarity triangle. Here our findings are as follows:

- The largest effects of new contributions for large  $\tan \bar{\beta}$  are seen in  $\Delta M_s$ . The corresponding contributions to  $\Delta M_d$  and  $\varepsilon$  are strongly suppressed either by inverse powers of  $\tan \bar{\beta}$  or by the smallness of  $d$ -quark mass.
- The dominant contributions to  $\Delta M_s$  for large  $\tan \bar{\beta}$  come from the operator  $Q_2^{\text{LR}} = (\bar{b}(1 - \gamma_5)s)(\bar{b}(1 + \gamma_5)s)$ . They originate from double penguin diagrams involving neutral Higgs particles and, to a lesser extent, in the box diagrams with charged Higgs exchanges. The dominant double penguin diagrams arise through the generation of flavour non-diagonal  $\tan \bar{\beta}$  enhanced couplings of neutral Higgs bosons to the down-type quarks and depend strongly on the mixing of the top squarks and their mass splitting.
- The contribution of double penguins grows like  $\tan^4 \bar{\beta}$  and interferes destructively with the SM contribution, suppressing considerably  $1 + f_s$  below unity.
- All these findings have the following phenomenological consequences. The MSSM with large  $\tan \bar{\beta}$ , substantial stop mixing and large stop mass splitting realizes the  $R_{sd} < 1$  scenario with  $\gamma < 90^\circ$  and generally smaller than in the SM and MFV models. As  $R_{d\varepsilon} = 1$  and  $1 + f_\varepsilon = 1$ , the lower bound  $\sin 2\beta > 0.50$  valid in the SM remains unchanged. Consequently if  $a_{\psi K_S}$  is found below 0.50, this scenario of the MSSM will be excluded (together with the SM) while other MSSM scenarios with lighter sparticles and lower  $\tan \bar{\beta}$ , belonging to the MFV class, may still be consistent with the data. As seen in fig. 4, for higher values of  $a_{\psi K_S}$  the MSSM scenario considered here is a vital possibility with the angle  $\gamma$  smaller than in the SM, although values of  $R_{sd}$  as low as 0.6 appear rather improbable.
- The constraint (2.18), which basically limits the magnitude of the stop mixing parameter  $A_t$ , has also important consequences for other processes involving the  $B^0$  mesons. For example, in the scenario considered in this paper, it severely limits possible enhancement of the  $B_{s,d}^0 \rightarrow \mu^+ \mu^-$  decay rate.

Detailed analysis of  $\Delta M_{d,s}$  and  $\varepsilon$  in the MSSM at large  $\tan \bar{\beta}$ , including also scenarios with light sparticles will be presented soon [26].

It will be exciting to watch future developments in the experimental values of  $\Delta M_s$ ,  $a_{\psi K_S}$  and the angle  $\gamma$  that will either choose one of the possibilities considered in this paper or constrain the parameters of GMFV models.

## Acknowledgments

A.J.B. and J.R. would like to thank Sebastian Jäger, Frank Krüger, Jörg Urban, Enrico Lunghi and Oscar Vives for useful discussions. The work of A.J.B. and J.R. was supported in part by the German Bundesministerium für Bildung and Forschung under the contract 05HT1WOA3. The work of P.H.Ch. was supported partially by the Polish State Committee for Scientific Research grant 5 P03B 119 20 for 2001-2002 and by the EC Contract HPRN-CT-2000-00148 for years 2000-2004. J.R. was also partially supported by the Polish State Committee for Scientific Research grant 2 P03B 060 18 for years 2000-2001.

## Appendix A

The four point loop functions with zero external momenta are defined as follows:

$$D_0(a, b, c, d) = \int \frac{d^4 k}{\pi^2} \frac{i}{[a][b][c][d]} = \frac{b}{(b-a)(b-c)(b-d)} \log \frac{b}{a} + \frac{c}{(c-a)(c-b)(c-d)} \log \frac{c}{a} + \frac{d}{(d-a)(d-b)(d-c)} \log \frac{d}{a} \quad (\text{A.1})$$

$$D_2(a, b, c, d) = \int \frac{d^4 k}{\pi^2} \frac{ik^2}{[a][b][c][d]} = \frac{b^2}{(b-a)(b-c)(b-d)} \log \frac{b}{a} + \frac{c^2}{(c-a)(c-b)(c-d)} \log \frac{c}{a} + \frac{d^2}{(d-a)(d-b)(d-c)} \log \frac{d}{a} \quad (\text{A.2})$$

where  $[a] \equiv k^2 - a$  etc. Finally,

$$H_2(x, y) = \frac{x \ln x}{(1-x)(x-y)} + \frac{y \ln y}{(1-y)(y-x)} . \quad (\text{A.3})$$

## References

- [1] A.J. Buras, *hep-ph/0101336*, lectures at the International Erice School, August, 2000.
- [2] B. Aubert et al., BaBar Collaboration, BABAR-PUB-01-18 (*hep-ex/0107013*).
- [3] K. Abe et al., Belle Collaboration, Belle Preprint 2001-10 (*hep-ex/0107061*).
- [4] T. Affolder et al., CDF Collaboration, *Phys. Rev.* **D61** (2000), 072005.
- [5] The ALEPH Collaboration, *hep-ex/0009058*.
- [6] LEP B-oscillation Working Group: [http://lepbosc.web.cern.ch/LEPBOSC/combined\\_results/](http://lepbosc.web.cern.ch/LEPBOSC/combined_results/).
- [7] A. Ali and D. London, *Eur. Phys. J.* **C9** (1999), 687; *Phys. Rep.* **320** (1999), 79; *hep-ph/0002167*; *Eur. Phys. J.* **C18** (2001), 665.
- [8] A.J. Buras, M.E. Lautenbacher and G. Ostermaier, *Phys. Rev.* **D 50** (1994), 3433.
- [9] A.J. Buras, P. Gambino, M. Gorbahn, S. Jäger and L. Silvestrini, *Phys. Lett.* **B500** (2001) 161.
- [10] A.J. Buras and R. Buras, *Phys. Lett.* **B501** (2001), 223.
- [11] M. Ciuchini, G. D'Agostini, E. Franco, V. Lubicz, G. Martinelli, F. Parodi, P. Roudeau and A. Stocchi, *hep-ph/0012308*; S. Plaszczynski and M.-H. Schune, *hep-ph/9911280*; A. Höcker, H. Lacker, S. Laplace and F. Le Diberder, *hep-ph/0104062*; S. Mele, talk Presented at *5<sup>th</sup> International Symposium on Radiative Corrections (RADCOR 2000)*, Carmel, California, September 2000, *hep-ph/0103040*.
- [12] B. Aubert et al., BaBar Collaboration, *hep-ex/0102030*.
- [13] G. Eyal, Y. Nir and G. Perez, *JHEP* **0008** (2000), 028.
- [14] J.P. Silva and L. Wolfenstein, *Phys. Rev.* **D63** (2001) 056001; A. Masiero, M. Piai and O. Vives, *hep-ph/0012096*.
- [15] A.L. Kagan and M. Neubert, *Phys. Lett.* **B492** (2000) 115.
- [16] Z.Z. Xing, *hep-ph/0008018*; H. Fritzsch and Z.Z. Xing, *hep-ph/0102295*.
- [17] R. Fleischer and Th. Mannel, *hep-ph/0101276*.
- [18] Y.-L. Wu and Y.-F. Zhou, *hep-ph/0102310*.

- [19] A. Masiero and O. Vives, *hep-ph/0104027*; A. Masiero, M. Piai, A. Romanino and L. Silvestrini, *hep-ph/0104101*.
- [20] S. Bergmann and G. Perez, *hep-ph/0103299*.
- [21] A. Ali and E. Lunghi, *hep-ph/0105200*.
- [22] M. Ciuchini, G. Degrassi, P. Gambino and G.-F. Giudice, *Nucl. Phys.* **B534** (1998), 3.
- [23] A.J. Buras and R. Fleischer, preprint TUM-HEP-412/01 (*hep-ph/0104238*).
- [24] M. Misiak, S. Pokorski and J. Rosiek, in *Heavy Flavours II*, eds. A.J. Buras and M. Lindner, World Scientific Publishing Co., Singapore 1998 (*hep-ph/9703442*).
- [25] A.J. Buras, P. Gambino, M. Gorbahn, S. Jäger and L. Silvestrini, *Nucl. Phys.* **B592** (2001), 55.
- [26] A.J. Buras, P.H. Chankowski, J. Rosiek and Ł. Sławianowska, in preparation.
- [27] A.J. Buras, M. Jamin, and P.H. Weisz, *Nucl. Phys.* **B347** (1990), 491.
- [28] J. Urban, F. Krauss, U. Jentschura and G. Soff, *Nucl. Phys.* **B523** (1998) 40.
- [29] M. Ciuchini, E. Franco, V. Lubicz, G. Martinelli, I. Scimemi and L. Silvestrini, *Nucl. Phys.* **B523** (1998) 501.
- [30] A.J. Buras, M. Misiak and J. Urban, *Nucl. Phys.* **B586** (2000), 397.
- [31] M. Ciuchini, et al., *JHEP* **9810** (1998), 008.
- [32] A.J. Buras, S. Jäger and J. Urban, *Nucl. Phys.* **B605** (2001), 600.
- [33] L. Wolfenstein, *Phys. Rev. Lett.* **51** (1983), 1945.
- [34] S. Herrlich and U. Nierste, *Nucl. Phys.* **B419** (1994), 292; *Phys. Rev.* **D52** (1995) 6505; *Nucl. Phys.* **B476** (1996), 27.
- [35] R. Fleischer, *Phys. Lett.* **B459** (1999), 306.
- [36] A.J. Buras and R. Fleischer, *Eur. Phys. J.* **C11** (1999) 93; *Eur. Phys. J.* **C16** (2000) 97; *hep-ph/0008298*.
- [37] X.-G. He, W.-S. Hou and K-Ch. Yang, *hep-ph/9902256*; W.-S. Hou and K.-Ch. Yang, *Phys. Rev.* **D61** (2000) 073014; W.-S. Hou, J.G. Smith and F. Würthwein, *hep-ex/9910014*.

- [38] M. Beneke, G. Buchalla, M. Neubert and C.T. Sachrajda, *hep-ph/0007256; hep-ph/0104110*;
- [39] D. Du, D. Yang and G. Zhu, *hep-ph/0005006*; T. Muta, A. Sugamoto, M.Z. Yang and Y.D. Yang, *hep-ph/0006022*.
- [40] M. Ciuchini, E. Franco, G. Martinelli, M. Pierini and L. Silvestrini, *hep-ph/0104126*.
- [41] C. R. Allton et al., *Phys. Lett.* **B453** (1999), 30.
- [42] J.A. Bagger, K.T. Matchev and R.J. Zhang, *Phys. Lett.* **B412** (1997), 77.
- [43] J. Flynn and C.-J.D. Lin, talk given at UK Phenomenology Workshop on Heavy Flavor and CP Violation, Durham, England, Sepember 2000, *hep-ph/0012154*; C.T. Sachrajda, *hep-lat/0101003*.
- [44] J. Rosiek, *Phys. Rev.* **D41** (1990), 3464, *Erratum hep-ph/9511250*.
- [45] P. Gambino and M. Misiak, preprint CERN-TH/2000-089 (*hep-ph/0104034*);
- [46] F. Blanc (the CLEO Collaboration), talk at the XXXVI<sup>th</sup> Rencontres de Moriond, March 2001, Les Arcs 1800, France.
- [47] P. Gambino, talk at the XXXVI<sup>th</sup> Rencontres de Moriond, March 2001, Les Arcs 1800, France.
- [48] E. Gabrielli and G.-F. Giudice, *Nucl. Phys.* **B433** (1995), 3.
- [49] N.H. Brown et al., *Phys. Rev. Lett.* **86** (2001), 2227.
- [50] G. Degrassi, P. Gambino and G.-F. Giudice, *JHEP* **0012** (2000), 009.
- [51] M. Carena, D. Garcia, U. Nierste and C.E.M. Wagner, *Phys. Lett.* **B499** (2001), 141.
- [52] P.H. Chankowski and S. Pokorski in *Perspectives on supersymmetry*, G.L. Kane ed., World Scientific Publishing Co., Singapore 1998 (*hep-ph/9707497*); M. Carena, U. Nierste and C.E.M. Wagner, *Nucl. Phys.* **B577** (2000), 88.
- [53] L.J. Hall, R. Rattazzi and U. Sarid, *Phys. Rev.* **D50** (1994) 7048.
- [54] C. Hamzaoui, M. Pospelov and M. Toharia, *Phys. Rev.* **D59** (1999), 095005.
- [55] K.S. Babu and C. Kolda, *Phys. Rev. Lett.* **84** (2000), 228.

- [56] P.H. Chankowski and L. Sławianowska *Phys. Rev.* **D63** (2001), 054012.
- [57] C. Bobeth, T. Ewerth, F. Krüger and J. Urban, preprint TUM-411/01, *hep-ph*/0104284.
- [58] C.-S. Huang, W. Liao, Q.-S. Yan and S.-H. Zhu, *Phys. Rev.* **D63** (2001), 114021, Erratum *ibid.* **D64** (2001), 059902.